Human Molecular Genetics, 2014, Vol. 23, No. 11 **3008–3023**
doi:10.1093/hmg/ddu011
Advance Access published on January 14, 2014

Interactions between Tau and α-synuclein augment neurotoxicity in a *Drosophila* model of Parkinson's disease

Bidisha Roy[1] and George R. Jackson[2,3,4,*]

[1]Mitchell Center for Neurodegenerative Diseases, [2]Department of Biochemistry and Molecular Biology, University of Texas Medical Branch Galveston, TX, USA and [3]Department of Neurology, Baylor College of Medicine, [4]Parkinson's Disease Research Education and Clinical Center, Michael E. DeBakey VA Medical Center, Room 2B-148C, 2002 Holcombe Boulevard, Houston, TX 77030, USA

Received December 12, 2013; Revised December 12, 2013; Accepted January 8, 2014

Clinical and pathological studies have suggested considerable overlap between tauopathies and synucleinopathies. Several genome-wide association studies have identified alpha-Synuclein (SNCA) and Tau (MAPT) polymorphisms as common risk factors for sporadic Parkinson's disease (PD). However, the mechanisms by which subtle variations in the expression of wild-type SNCA and MAPT influence risk for PD and the underlying cellular events that effect neurotoxicity remain unclear. To examine causes of neurotoxicity associated with the α-Syn/Tau interaction, we used the fruit fly as a model. We utilized misexpression paradigms in three different tissues to probe the α-Syn/Tau interaction: the retina, dopaminergic neurons and the larval neuromuscular junction. Misexpression of Tau and α-Syn enhanced a rough eye phenotype and loss of dopaminergic neurons in fly tauopathy and synucleinopathy models, respectively. Our findings suggest that interactions between α-Syn and Tau at the cellular level cause disruption of cytoskeletal organization, axonal transport defects and aberrant synaptic organization that contribute to neuronal dysfunction and death associated with sporadic PD. α-Syn did not alter levels of Tau phosphorylated at the AT8 epitope. However, α-Syn and Tau colocalized in ubiquitin-positive aggregates in eye imaginal discs. The presence of Tau also led to an increase in urea soluble α-Syn. Our findings have important implications in understanding the cellular and molecular mechanisms underlying α-Syn/Tau-mediated synaptic dysfunction, which likely arise in the early asymptomatic phase of sporadic PD.

INTRODUCTION

Tau, a highly soluble microtubule-associated protein, has been linked to tauopathies, including Alzheimer's disease (AD) (1,2). α-Syn has been implicated in the pathogenesis of Parkinson's disease (PD) (3). Although they traditionally are associated with different syndromes, pathological and genetic studies have suggested a strong association between tauopathies and synucleinopathies. α-Syn-immunoreactive structures (4–8), including Lewy bodies (LBs) (9–12), have been found in sporadic and familial AD brain. Tau-immunoreactive LB have been detected in the brain of sporadic PD and dementia with Lewy body (DLB) patients (13,14). Genome-wide association studies (GWAS) have also confirmed polymorphisms in alpha-Synuclein (SNCA) and Tau (MAPT) as common risk factors for PD (15,16). However, the mechanisms by which variations in SNCA and MAPT influence risk for PD are unknown (17).

A few reports have shed light on the mechanistic underpinnings of neurotoxicity in the α-Syn/Tau interaction. Neurotoxic MPP^+ (1-methyl-4-phenylpyridinium ion) induces Tau hyperphosphorylation in the presence of α-Syn in SY5Y neuroblastoma cells (18) and wild-type mice (19). Sidhu and coworkers found that α-Syn contributes to GSK-3β-catalyzed Tau phosphorylation in various models of parkinsonism (20,21). Giasson and coworkers reported that α-Syn induces fibrillization of Tau and that coincubation of Tau and α-Syn synergistically promotes fibrillization of both proteins (22). Kotzbauer and coworkers reported the formation of insoluble filamentous α-Syn and Tau in A53T α-Syn PD

*To whom correspondence should be addressed at: Parkinson's Disease Research Education and Clinical Center, Michael E. DeBakey VA Medical Center, Room 2B-148C, 2002 Holcombe Boulevard, Houston, TX 77030, USA. Tel: +1 7137948936; Fax: +1 7137948888. Email: grjackso@bcm.edu; George.Jackson6@va.gov

brain (23). Both of these efforts suggest that distinct amyloidogenic proteins may cross-seed each other in neurodegenerative diseases and thereby enhance disease intensity and accelerate its progression.

To examine further putative causes of synergistic toxicity of α-Syn/Tau, we used the genetically tractable model organism *Drosophila*. By utilizing misexpression paradigms in three different tissues: the retina (using the pan-retinal *glass* (*gl*) promoter), dopaminergic neurons (under control of the tyrosine hydroxylase promoter) and in the larval neuromuscular junction (NMJ) using motor neuron drivers (OK6 and VGLUT), we probed the affected cellular processes that lead to neurotoxicity. Misexpression of α-Syn with Tau enhanced a rough eye phenotype, loss of dopaminergic neurons and motor dysfunction in adults. Widespread cytoskeletal disorganization in the eye and abnormal microtubule organization in the larval neuromuscular junction were observed when both proteins were coexpressed. Misexpression of these proteins also led to axonal transport defects, decreased presynaptic proteins (Synapsin and Bruchpilot) and synaptic apposition defects. α-Syn did not alter levels of Tau phosphorylated at the AT8 epitope. However, α-Syn and Tau were observed to coexist in ubiquitin positive aggregates in the eye imaginal disc. Furthermore, Tau increased α-Syn in the urea fraction of sequential protein extracts. Our findings suggest that interactions between α-Syn and Tau at the cellular level cause disruption of cytoskeletal organization, axonal transport defects and aberrant synaptic organization that contribute to neuronal dysfunction and death associated with sporadic PD.

RESULTS

Misexpression of α-Syn enhances the Tau-mediated rough eye phenotype and apoptotic cell death in the eye

We misexpressed wild-type human α-Syn (24) in the *Drosophila* eye using the GMR-GAL4 driver in combination with human wild-type full-length (2N/4R) tau using a *gl*-Tau construct (human tau cDNA fused directly to the eye-specific *gl* promoter; (25)). *gl*-Tau misexpression causes a rough phenotype of the external eye associated with abnormalities of photoreceptor neurons and other cell types in the underlying retina (26). In the *gl*-Tau flies, the degree of the rough eye phenotype is intermediate and more pronounced anteriorly. The phenotype caused by misexpression of α-Syn alone (Fig. 1F) was indistinguishable from that of the driver (Fig. 1E). On the other hand, human Tau resulted in rough, reduced eyes, with the posterior region of the eye remaining more normal (Fig. 1G). Misexpression of both Tau and α-Syn resulted in a more severe rough eye, with the abnormal phenotype extending farther posteriorly (Fig. 1H). We also expressed a non-toxic protein (green fluorescent protein; GFP) along with Tau to rule out non-specific effects. Coexpression of Tau and GFP did not alter the eye phenotype of the *gl*-Tau flies (Fig. 1D). Three-dimensional reconstruction of the adult eye aids in assessment of eye phenotypes (25,27). Peaks and valleys are two morphological contours of the 3D eye; peaks represent the normal organization of the photoreceptor neurons and other cell types underlying the retina. On the other hand, any form of abnormality in this organization results in collapse of the retina, leading to the formation of valleys. Eyes of animals coexpressing Tau and α-Syn (Fig. 1P) were more flattened than those expressing Tau alone (Fig. 1O). Both the wild-type (driver alone; Fig. 1M) and the α-Syn flies (Fig. 1N) had eyes with a larger volume raised above the cuticular surface. Coexpression of the non-toxic protein GFP along with Tau (Fig. 1L) showed retinal 3D volumetric morphology comparable with the eyes expressing Tau alone (Fig. 1K). Wild-type (Fig. 1I) and GFP (Fig. 1J) eyes were indistinguishable. These results confirm that the interaction between Tau and α-Syn is specific, as the presence of a non-toxic protein did not alter the phenotypic readout of Tau.

We previously showed (26) that expressing two copies of the Tau transgene in the larval eye disc results in cell death as assessed by abnormal accumulation of lamin, an indicator of nuclear envelope breakdown, which in turn is one of the hallmarks of apoptosis. To assess neurotoxicity associated with the α-Syn/Tau interaction, we stained the larval eye disc with an antibody against cleaved caspase-3 (activated caspase-3). This antibody has been widely used as a marker for dying cells (28–30). Neither the controls (Fig. 2A) nor the α-Syn eye discs (Fig. 2B) showed appreciable cleaved caspase-3 activity. Flies misexpressing Tau showed activated caspase-3 activity posterior to the morphogenetic furrow (Fig. 2C). Coexpression of Tau and α-Syn led to increased activated caspase-3 (Fig. 2D).

Misexpression of α-Syn enhances Tau-induced motor dysfunction

Motor behavior has been used to interrogate neuronal function in various neurodegenerative models. Tau has previously been implicated in axonal transport defects and locomotor dysfunction in a *Drosophila* model (31). To examine whether coexpression of α-Syn and Tau modulates adult locomotor behavior, we used the pan neuronal *elav*-GAL4 driver to express Tau, α-Syn or both in postmitotic neurons. We tested motor behavior using a simple climbing assay (negative geotaxis) in which a single adult male (7 days posteclosion) is tapped to the bottom and allowed to climb up an empty vial for 10 s. The distance travelled by the individual fly within the given time frame is a measure of its motor performance or climbing index. Motor performance of flies expressing α-Syn alone was indistinguishable from their control counterparts ($P = 0.64$). On the other hand, flies expressing Tau had severe motor deficits, with an ∼67% decrease in the climbing index. The motor behavior was further impaired by 88% when compared with control with coexpression of Tau and α-Syn (Fig. 3).

Coexpression of Tau and α-Syn leads to cytoskeletal disorganization and abnormal microtubule organization

Both Tau and α-Syn have been reported to function as microtubule-binding proteins (32,33) and bind the actin cytoskeleton (34–39). We examined actin and tubulin bundles along rhabdomere shafts in adult retinal longitudinal preparations. Misexpression of Tau (Fig. 4C) and α-Syn (Fig. 4B) alone did not lead to any dramatic change in the organization of actin bundles in rhabdomeres. However, phalloidin (an F-actin marker) staining of the retinal preparations of GMR-GAL4/+, *gl*-Tau/+; UAS-α-Syn/+ flies showed highly disorganized actin bundles (Fig. 4D). Anti-tubulin staining of the retinal sections showed an organized rod-like staining pattern of tubulin in

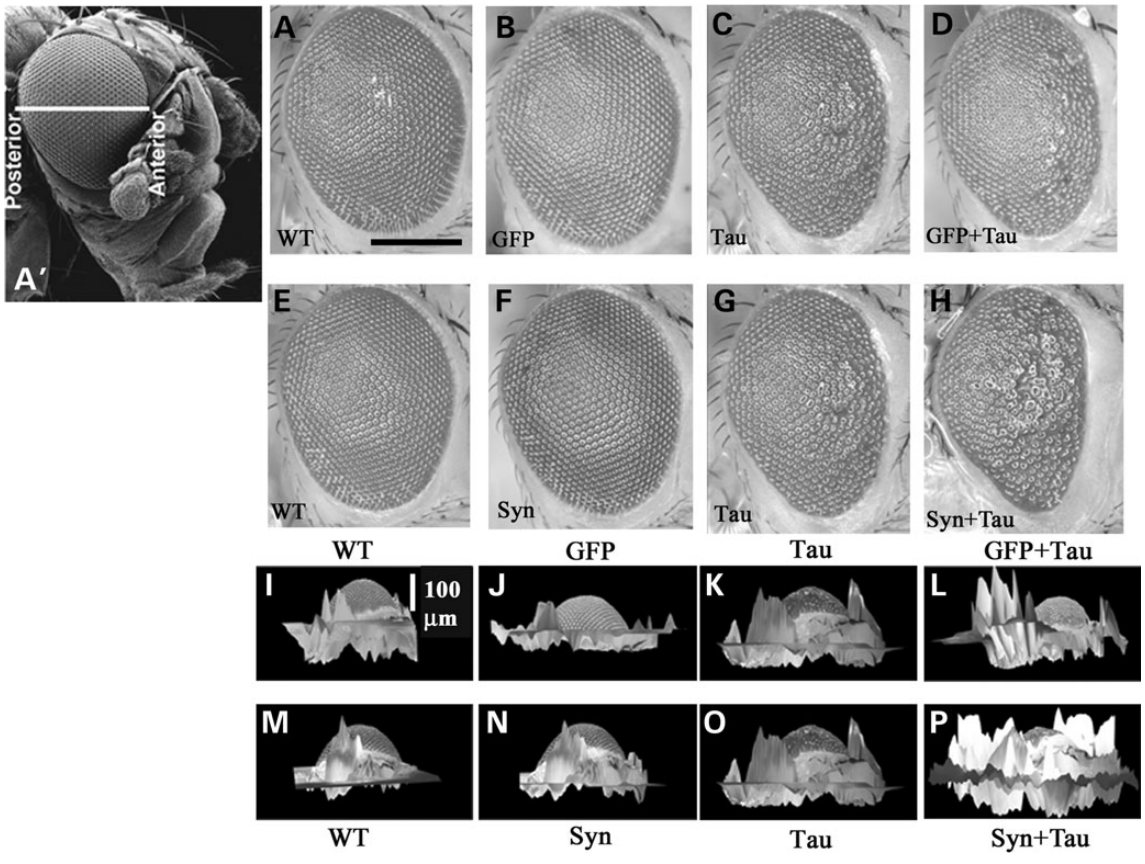

Figure 1. Misexpression of α-Syn enhances the Tau-mediated eye phenotype. (**A′**) Scanning EM of the adult *Drosophila* eye showing the anterior–posterior axis. Light micrographs (**A**–**H**) and three-dimensional reconstructed images (**I**–**P**); stacks were generated at 10 μm intervals. Misexpression of GFP did not alter Tau-induced toxicity (A–D; I–L), whereas α-Syn enhances Tau toxicity (E–H; M–P). Genotypes: GMR-GAL4/+ (A, E, I, M), GMR-GAL4/+; +; UAS-GFP/+ (B, J), GMR-GAL4/+; +; UAS-Syn/+ (F, N), GMR-GAL4/+; *gl*-Tau/+ (C, G, K, O), GMR-GAL4/+; *gl*-Tau/+; UAS-GFP/+ (D, L), GMR-GAL4/+; *gl*-Tau/+; UAS-Syn/+ (H, P). Scale bar: 100 μm.

the wild-type (Fig. 4E) and the α-Syn (Fig. 4F)-expressing flies. The microtubule shafts were disorganized in the Tau misexpressing flies (Fig. 4G) and the extent of this disorganization was enhanced in the Tau/α-Syn coexpressing transgenics (Fig. 4H).

We further characterized the extent of cytoskeletal disorganization due to the coexpression of Tau and α-Syn using microtubule unbundling phenotypes in the larval neuromuscular junction. Using the monoclonal antibody 22C10, which recognizes Futsch, a presynaptic microtubule-associated protein related to vertebrate MAP-1B (40), others have shown cytoskeletal disorganization (41) and microtubule unbundling (42). The pattern of Futsch staining at the neuromuscular junction has been extensively characterized (40,43,44). In wild-type larvae, Futsch staining in most boutons appears thread like, running along the axis of each synaptic branch and continuous with the axonal cytoskeleton. In some cases, highly organized loops are also observed within distal synaptic boutons; these have been correlated with microtubule stability or lack of change, whereas disruption of these loops is associated with motility and plasticity (40,44). Occasionally, there might be a few distal boutons in which Futsch staining appears punctate or diffuse in the wild-type animals (41,44). Futsch staining can also be found to fill the entire presynaptic space (filled phenotype) (41) or form many thin filaments diverging from the central bundle in a disorganized and spread out pattern within the bouton (splayed phenotype) (44). These forms of Futsch staining (diffuse, punctate, splayed and filled) have been described as variant forms of disorganized microtubules found in mutants affecting synaptic structure. We have referred to the boutons having these variant forms of Futsch staining as abnormal boutons, in contrast with those boutons with a filamentous, thread-like staining pattern, which we consider normally bundled boutons. To determine if coexpression of Tau and α-Syn leads to disorganization of microtubules, we examined the pattern of Futsch staining at the neuromuscular junction of larvae and quantitated the percentage of abnormal boutons. In the control animals, ∼11% of the boutons were abnormal (Fig. 4I, M and Q). In animals misexpressing α-Syn, 21% of the boutons showed the unbundled phenotypes (Fig. 4J, N and Q). In contrast, Tau induced a substantial increase in the number of abnormal boutons (35%; Fig. 4K, O and Q). Coexpression of Tau and α-Syn further increased the number of boutons with disorganized microtubules to 60% (Fig. 4L, P and Q).

Misexpression of α-Syn enhances Tau-mediated axonal transport defects

Axonal and cytoplasmic accumulation of proteins and organelles are pathological hallmarks of human neurodegenerative

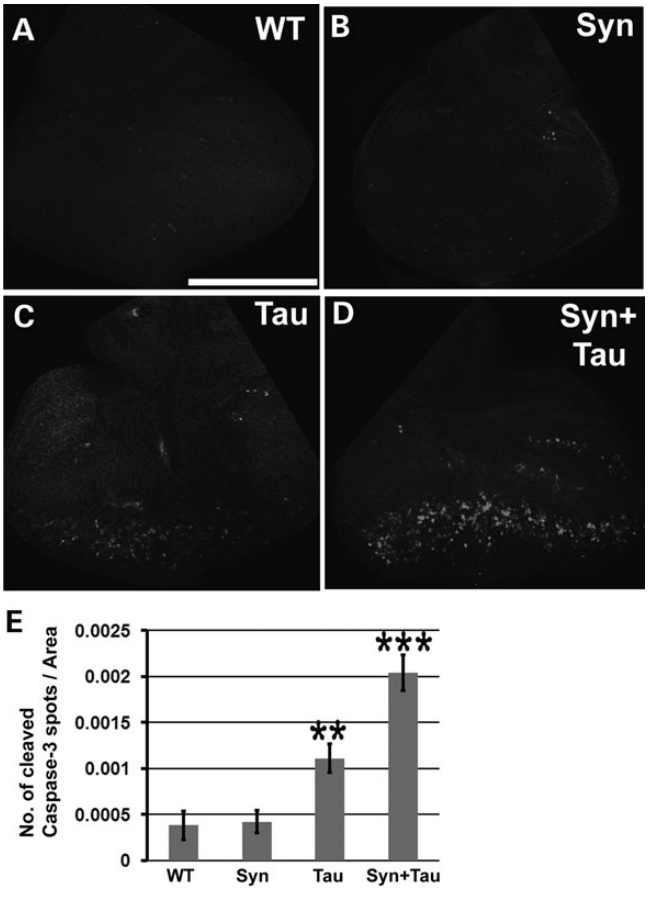

Figure 2. Misexpression of α-Syn enhances Tau-mediated cleaved caspase-3 activity. (**A**–**D**) Z-stacked confocal images of third instar larval eye discs stained with antibody against cleaved caspase 3. (**E**) Bar graph representing the number of cleaved caspase 3 puncta. *Y*-axis represents the total number of cleaved Caspase 3 spots/area. Values on the *Y*-axis represent mean ± SEM. *X*-axis represents the various genotypes. $^{**}P < 0.01$; $^{***}P < 0.05$ using one-way ANOVA + Fisher LSD multiple comparison test. Genotypes: (A) GMR-GAL4/+ ($N = 7$, *Y*-axis value = 0.00038), (B) GMR-GAL4/UAS-lacZ; UAS-Syn/+ ($N = 7$, *Y*-axis value = 0.00041), (C) GMR-GAL4, UAS-Tau/+; UAS-lacZ/+ ($N = 10$, *Y*-axis value = 0.00111) and (D) GMR-GAL4, UAS-Tau/+; UAS-Syn/+ ($N = 10$, *Y*-axis value = 0.00204). Scale bar: 170 μm.

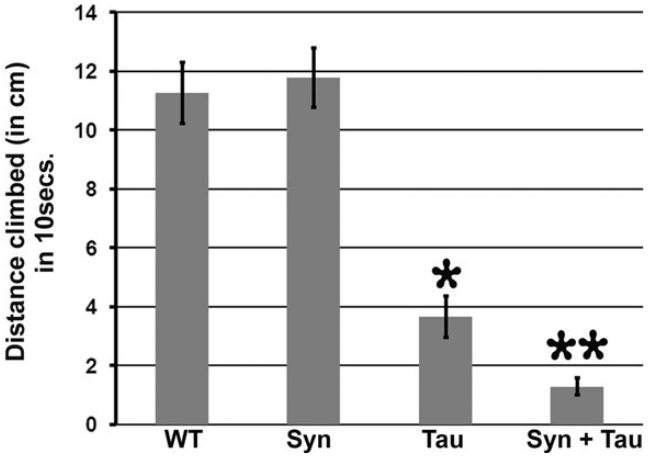

Figure 3. Misexpression of α-Syn enhances Tau-induced motor dysfunction. Using the pan-neuronal-driver C155-GAL4, both Tau alone and Syn + Tau demonstrate impairments in climbing performance when compared with control and α-Syn flies. However, the extent of this motor impairment is higher (~3-fold) in the α-Syn/Tau flies. Bar graphs representing single fly motor behavior. The *Y*-axis represents the distance climbed by a 7-day-old male fly in 10 s. Values on the *Y*-axis represent mean ± SEM. $^{**}P < 0.01$; $^{*}P < 0.05$ using one-way ANOVA + Fisher LSD correction for multiple comparisons. Genotypes: (**A**) WT: C155-GAL4/+ ($N = 9$, *Y*-axis value = 11.26), (**B**) Syn: C155-GAL4/+; UAS-lacZ/+; UAS-Syn/+ ($N = 11$, *Y*-axis value = 11.78), (**C**) Tau: C155-GAL4/+; UAS-Tau/+; UAS-lacZ/+ ($N = 9$, *Y*-axis value = 3.67) and (**D**) Syn + Tau: C155-GAL4/+; UAS-Tau/+; UAS-Syn/+ ($N = 12$, *Y*-axis value = 1.29).

diseases. Axonal swellings and spheroids have been described in a number of neurodegenerative diseases (45). *In vitro* studies have shown that tau interferes with kinesin activation and disrupts the transport of various kinesin cargoes (46–48). Lovestone and coworkers reported that overexpression of human tau disrupts axonal transport, causing vesicle aggregation and locomotor dysfunction (31). Parmentier and colleagues have shown that overexpression of wild-type Tau (0N4R), hypophosporylatable Tau (Tau AP) and pseudophosphorylated Tau (Tau E14) all lead to vesicular clogging indicative of axonal transport defects (49). Protein accumulation in the axon is an indication of axonal transport defects. Accumulation of synaptic vesicle proteins including synaptotagmin and cysteine string protein (50,51) has been routinely used to assay axonal transport defects. Additionally, staining the axons with an antibody against Bruchpilot (BRP; an active zone marker, the *Drosophila* homolog of CAST protein important for active zone assembly) (52) and DVGLUT (a synaptic vesicle-associated protein) (53) have been used to detect axonal traffic jams.

To examine the effects of α-Syn/Tau on axonal transport, we assessed axonal accumulations of DVGLUT. The motor neuron-specific enhancer trap lines OK6- and VGLUT-GAL4 were used to drive expression of Tau and/or α-Syn. DVGLUT accumulates in motor neuron axons leading to the formation of axonal traffic jams. Flies expressing Tau alone showed some increase in the number of these aggregates (Fig. 5C) with respect to their control (Fig. 5A) and α-Syn (Fig. 5B)-expressing counterparts. Although we observed a few axonal aggregates in the α-Syn misexpressing animals, the number was not significantly different when compared with the driver alone ($P = 0.28$; Fig. 5E). The number of DVGLUT aggregates $>1.68\ \mu m^2$ approximately doubled in animals coexpressing Tau and α-Syn when compared with the Tau misexpressing animals (Fig. 5D and E). The axonal transport defect due to α-Syn/Tau also was apparent using accumulation of BRP in the dual α-Syn/Tau transgenics (Supplementary Material, Fig. S1).

Misexpression of Tau enhances α-Syn-mediated dopaminergic neuronal loss

Loss of dopaminergic neurons in the dorsomedial and dorsolateral (DL) clusters have been characterized in fly PD models. We confirmed a decrease in TH immunoreactive cells in the DL cluster at 6 weeks in TH-GAL4, UAS-α-Syn/+; TH-GAL4, UAS-α-Syn/+ (Fig. 6C and E) transgenic flies when compared with their control counterparts (TH-GAL4/+ flies; Fig. 6A). Overexpression of Tau, on the other hand, did not lead to significant cell loss ($P = 1$; Fig. 6B and E). However, misexpression of

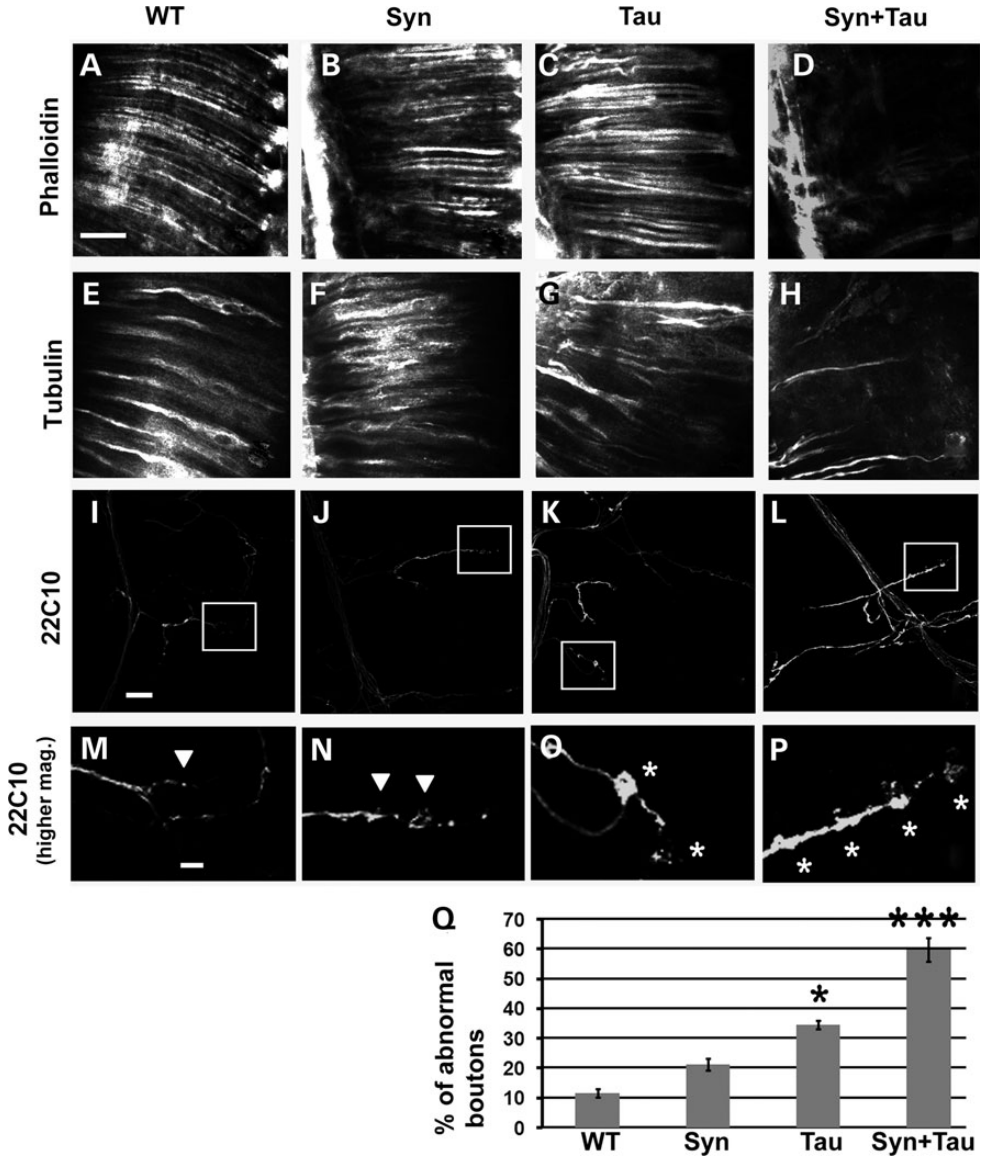

Figure 4. Coexpression of Tau and α-Syn leads to cytoskeletal disorganization and abnormal microtubule organization. Confocal images of retinal longitudinal sections stained with phalloidin (**A**–**D**) and tubulin antibody (**E**–**H**). Genotypes: GMR-GAL4/+ (WT: A, E), GMR-GAL4/+; +; UAS-Syn/+ (Syn: B, F), GMR-GAL4/+; *gl*-Tau/+ (Tau: C, G), GMR-GAL4/+; *gl*-Tau/+; UAS-Syn/+ (Syn + Tau: D, H). (**I**–**P**) Representative confocal images of synapses on muscle 4 of *OK6*-GAL4/+ (I, M), *OK6-GAL4*/UAS-lacZ; UAS-Syn/+ (J, N), *OK6-GAL4*/UAS-Tau; UAS-lacZ/+ (K, O) and OK6-GAL4/UAS-Tau; UAS-Syn/+ (L, P) animals stained with anti-Futsch (22C10). Anti-Futsch labels stable presynaptic microtubules. (M)–(P) represent zoomed images of the boxed regions in (I)–(L), respectively. (**Q**) Quantitation of microtubule morphology assessed using anti-Futsch. The percentage of boutons of the muscle 4 synapse exhibiting disorganized microtubule phenotypes (abnormal boutons) was calculated. Boutons with unorganized microtubules have been represented with white asterisks in (O) and (P) and boutons with organized microtubules have been marked by white arrowheads in (M) and (N). *Y*-axis on the bar graph represents percentage of abnormal boutons. [*Y*-axis values − WT (*OK6*-GAL4/+): 11%, Syn (*OK6-GAL4*/UAS-lacZ; UAS-Syn/+): 21%, Tau (*OK6-GAL4*/UAS-Tau; UAS-lacZ/+): 35% and Syn + Tau (OK6-GAL4/UAS-Tau; UAS-Syn/+): 60%]. $N = 12$ synapses across six animals; $^{***}P < 0.001$; $^{*}P < 0.01$ using one-way ANOVA + Fisher LSD test. Scale bar: (A)–(L), 20 μm; (I)–(L) and (M)–(P), 5 μm.

α-Syn and Tau enhanced dopaminergic cell loss in the DL cluster of TH-GAL4, UAS- α-Syn/UAS-Tau; TH-GAL4, UAS-α-Syn/+ flies (Fig. 6D and E). Tau levels were comparable between UAS-Tau/+; TH-GAL4/+ and TH-GAL4, UAS-α-Syn/UAS-Tau; TH-GAL4, UAS-α-Syn/+ flies. On the other hand, driving expression of Tau using two copies of the TH GAL4 driver increased mRNA expression by 10-fold when compared with TH-GAL4, UAS-α-Syn/UAS-Tau; TH-GAL4, UAS-α-Syn/+ flies (data not shown). This is due to titration effects associated with imbalance in the number of GAL4 and UAS copies. The lack of a TH-GAL4, UAS-lacZ; TH-GAL4, UAS-lacZ transgenic line had to be bypassed by using the UAS-Tau/+; TH-GAL4/+ trangenic. In the TH-GAL4, UAS-α-Syn/UAS-Tau; TH-GAL4, UAS-α-Syn/+ transgenic, two copies of GAL4 drive expression of three copies of UAS, so that one UAS is driven by 67% of the GAL4. On the other hand, in UAS-Tau/+; TH-GAL4/+, one UAS is driven by one GAL4. In the TH-GAL4/UAS-Tau; TH-GAL4/+ transgenics, one UAS is driven by two copies of GAL4, leading to very high levels of Tau.

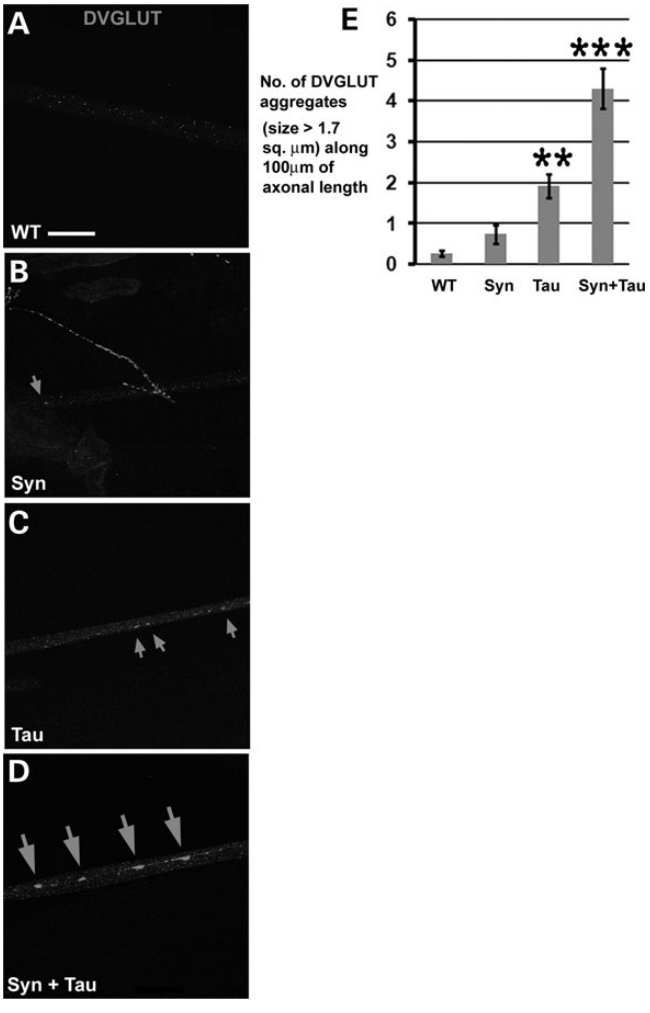

Figure 5. Misexpression of α-Syn enhances Tau-mediated axonal transport defects. (**A**–**D**) Immunostaining of larval segmental nerves with antibody against DVGLUT. Confocal images of axons in the distal (with respect to the ventral nerve chord)/posterior regions of the segmental nerve (A5–A6 segments) showing accumulation of DVGLUT-positive axonal aggregates (arrows). The extent of accumulation of DVGLUT aggregates is higher in the VGLUT^{OK371}-GAL4/UAS-Tau; UAS-Syn/+ animals in comparison with the VGLUT^{OK371}-GAL4/UAS-Tau; UAS-lacZ/+ animals. VGLUT^{OK371}-GAL4/UAS-lacZ; UAS-Syn/+ animals show few axonal aggregates and are indistinguishable from controls. (**E**) Bar graph representing DVGLUT accumulation in axons. *Y*-axis: number of DVGLUT aggregates of $>1.7\ \mu m^2$ along 100 μm of axonal length. Number of animals tested: 7 per genotype. Genotypes: (A) WT: VGLUT^{OK371}-GAL4/+ [*Y*-value: 0 aggregates per 100 μm], (B) Syn: VGLUT^{OK371}-GAL4/UAS-lac Z; UAS-Syn/+ [*Y*-value : ∼1 aggregate per 100 μm], (C) Tau: VGLUT^{OK371}-GAL4/UAS-Tau; UAS-lacZ [*Y*-value : 2 aggregates per 100 μm] and (D) Syn + Tau: VGLUT^{OK371}-GAL4/UAS-Tau; UAS-Syn/+ [*Y*-value: 4 aggregates per 100 μm]. $^{***}P < 0.001$; $^{**}P < 0.01$; one-way ANOVA + Fisher test. Scale bar: (A–D), 20 μm.

Coexpression of α-Syn and Tau leads to synaptic defects in the neuromuscular junction

Synaptic α-Syn pathology is one of the main contributors to neurodegeneration (54). In DLB, 90% of α-Syn aggregates are presynaptic, suggesting that aggregate-based synaptic dysfunction may be one cause of neurodegeneration (54,55). α-Syn controls synaptic membrane processes and biogenesis, interacts with and modulates expression and distribution of synaptic proteins and controls neurotransmitter release (56–68). Tau, on the other hand, plays a role in microtubule assembly, axonal transport, neurite outgrowth and stability of microtubules (69). Missorting of Tau and loss of synapses are early events in AD. Tau causes decreased postsynaptic (PSD95, neuroligin, AMPA and NMDA receptors) and presynaptic proteins (bassoon and piccolo), mitochondrial dysfunction and loss of spines in mature hippocampal neurons (70). Oligomeric Tau induces synaptic dysfunction by reducing levels of the synaptic vesicle-associated proteins synaptophysin and septin-11 (71). Overexpression of human Tau in *Drosophila* larval motor neurons causes morphological and functional abnormalities in the NMJ (72). Tau-expressing NMJ have irregular and abnormal bouton structures, abnormal endo- and exocytosis, and reduced evoked synaptic potentials (72). However, the effect of misexpressing both Tau and α-Syn on synaptic organization has not been clearly elucidated. Using the motor neuron-specific-driver OK6-GAL4, we examined effects of α-Syn/Tau on expression of the vesicle clustering protein synapsin. Single bouton analysis revealed a decrease in synapsin in the α-Syn flies (Fig. 7C, G and I). These data are consistent with the observation of Edwards *et al*. (68) that α-Syn overexpression reduces synapsin-1, thus impairing vesicle reclustering after exocytosis. *Drosophila* synapsin is known to maintain vesicle clustering over the periphery of the bouton (73). Overexpression of Tau also resulted in decreased endogenous synapsin (Fig. 7B, C and I). Coexpression of Tau and α-Syn led to a further 2-fold decrease in synapsin when compared with either alone (Fig. 7D, H and I).

We also examined expression of BRP, the *Drosophila* homolog of the human AZ protein ELKS/CAST/ERC, which is required for structural integrity and function of synaptic active zones (52). Quantification of BRP puncta in a single bouton of the A2 hemisegment of muscle IV relative to the bouton's cross-sectional area showed a decrease for Tau misexpressing transgenics (Supplementary Material, Fig. S2G, I and M). No change was observed in the animals expressing α-Syn (Supplementary Material, Fig. S2D, F and M) with respect to controls. However, coexpression of Tau and α-Syn led to a further reduction in the number of BRP-positive puncta in a single bouton (Supplementary Material, Fig. S2J, L and M) when compared with the Tau alone flies.

We further examined synaptic defects, which have been reported previously in a fly AD model (74). α-Syn led to increased unapposed *Drosophila* glutamate receptor type III (DGluRIII; Fig. 7K and N) when compared with controls. In normal synapses, presynaptic BRP puncta sit tightly apposed to the postsynaptic DGluRIII puncta. Abnormalities in this kind of synaptic organization are attributed to the increase in the presence of unopposed glutamate receptors, which lack opposite active zone partners. There was also an increase in the number of unapposed DGluRIII in the animals misexpressing Tau (Fig. 7L and N). However, coexpression of Tau and α-Syn led to a further increase in the percentage of unopposed glutamate receptors when compared with the Tau- or α-Syn-expressing animals (Fig. 7M and N).

Localization of Tau and α-Syn in dual transgenics

Neuronal colocalization of Tau and α-Syn has been reported in familial AD, Down's syndrome and DLB brain (6,12,13,75). Dual staining of the striatum of PDGF-α-Syn mice with antibodies to α-Syn and p-Tau shows strong colocalization (21). The larval eye disc has been routinely used to check for compartmental

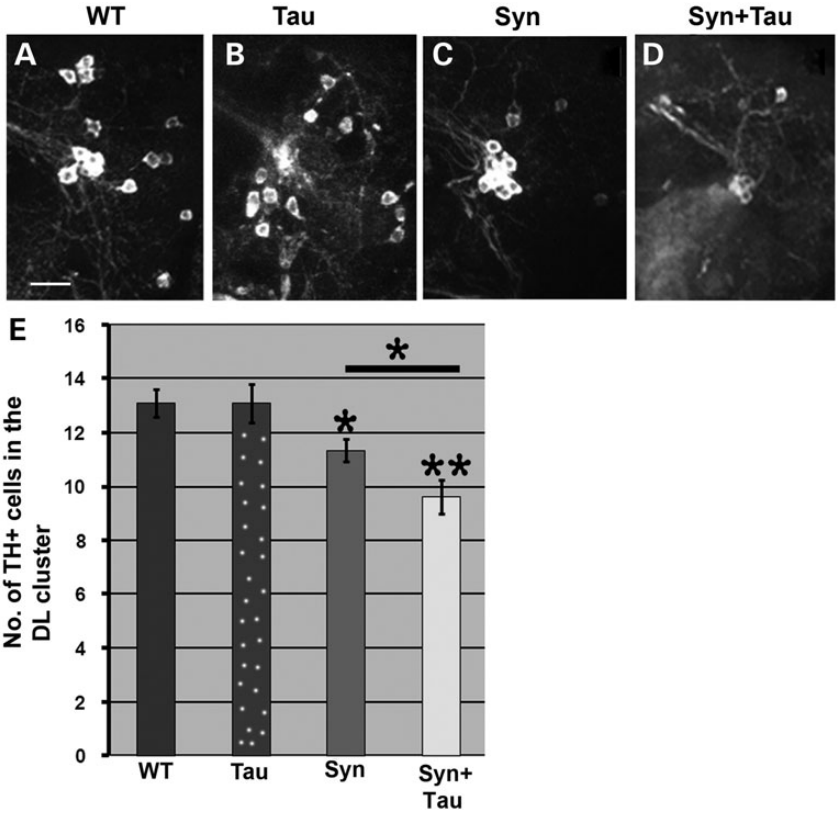

Figure 6. Tau misexpression enhances α-Syn-mediated dopaminergic cell loss. (**A**–**D**) Confocal images from 6-week-old adult fly brains immunostained with anti-TH (tyrosine hydroxylase) to mark DA neurons. The images represent the dopaminergic neurons in the DL (dorsolateral) cluster. (**E**) Bar graph representing the total number of TH-positive neurons on the *Y*-axis. Genotypes: (A/WT): TH-GAL4/+ [*Y*-axis value: 13]; (B/Tau): UAS-Tau/+; TH-GAL4/+ [*Y*-axis value: 13]; (C/Syn): TH-GAL4, UAS-Syn/+; TH-GAL4, UAS-Syn/+ [*Y*-axis value, 11] ; (D/Syn + Tau): TH-GAL4, UAS-Syn/UAS-Tau; TH-GAL4, UAS-Syn/+ [*Y*-axis value: 9]. $N = 11$. $^{*}P < 0.05$; $^{**}P < 0.01$; one-way ANOVA + Fisher test. Scale bar: (A–D), 15 μm.

localization of various proteins (76). We performed triple staining of eye discs with antibodies against Tau (T-46), α-Syn (rabbit polyclonal AB5038) and Elav (a nuclear marker; Fig. 8A–J). Confocal images of single planar sections of third instar larval eye discs from the GMR-GAL4/UAS-Tau; UAS Syn/+ double transgenics stained with Tau, α-Syn and nuclear antibodies showed strong cytoplasmic colocalization (Fig. 8E–J).

Abnormal aggregation of cellular proteins is a common feature of many neurodegenerative diseases, including AD, Huntington's disease, PD, prion disorders and amyotrophic lateral sclerosis (77–81). In PD, Tau and α-Syn colocalize in Lewy bodies (14). Triple staining of eye discs from the GMR-GAL4/UAS-Tau; UAS-α-Syn/+ larvae using antibodies against Tau, α-Syn and ubiquitin showed α-Syn and Tau-positive puncta throughout the cytoplasm along with more diffuse staining (Fig. 8K, L and N). Anti-ubiquitin staining confirmed these puncta to be ubiquitinated (Fig. 8M and N). These results are consistent with the theme of Tau coaggregation with α-Syn under pathophysiological conditions.

We also stained larval fillet preparations of animals coexpressing Tau and α-Syn with mouse T-46 (Tau specific; Fig. 8O), rabbit AB 5038 (α-Syn specific; Fig. 8P) and horseradish peroxidase (HRP) antibodies; Tau and α-Syn largely colocalized in the axons of motor neurons (Fig. 8Q, R and S). This observation is consistent with a proposed interaction between Tau and α-Syn in modulating axonal functions, e.g. transport. We also stained the larval NMJ; although α-Syn staining was enriched in the presynaptic compartment of boutons stained with HRP (Fig. 8U and W), Tau was not found at the NMJ (Fig. 8T and W).

Mechanisms underlying α-Syn/Tau-mediated toxicity

MPP^{+} induces hyperphosphorylation of Tau in the presence of colocalizing α-Syn in SY5Y neuroblastoma cells (18), primary mesencephalic neurons and wild-type mice (19). Furthermore, Sidhu and coworkers (20) reported that the phosphorylation of Tau by α-Syn in various toxin-derived models of parkinsonism is mediated by GSK-β. Coimmunoprecipitation studies revealed that α-Syn, pSer396/404-Tau and p-GSK-β exist as a heterotrimeric complex in SY5Y cells. In the A53T α-Syn transgenic mouse, Sidhu and coworkers (82) found elevated levels of α-Syn in the striatum, increased hyperphosphorylated Tau and increased activated p-GSK-β. To assess whether misexpression of α-Syn leads to any change in the p-Tau (pSer202/pThr205) levels in our model of α-Syn/Tau interaction, we performed immunoblots with head extracts. We probed the blot with AT8, a monoclonal antibody that recognizes Tau phosphorylated at serine 202 and threonine 205, T-46, which detects total Tau, and GAPDH as a loading control. We did not detect any differences in AT8 signal between Tau alone and dual Tau/α-Syn transgenics ($P = 0.974$; Fig. 9A and B). Total Tau levels were comparable in these animals (Fig. 9C). Differential

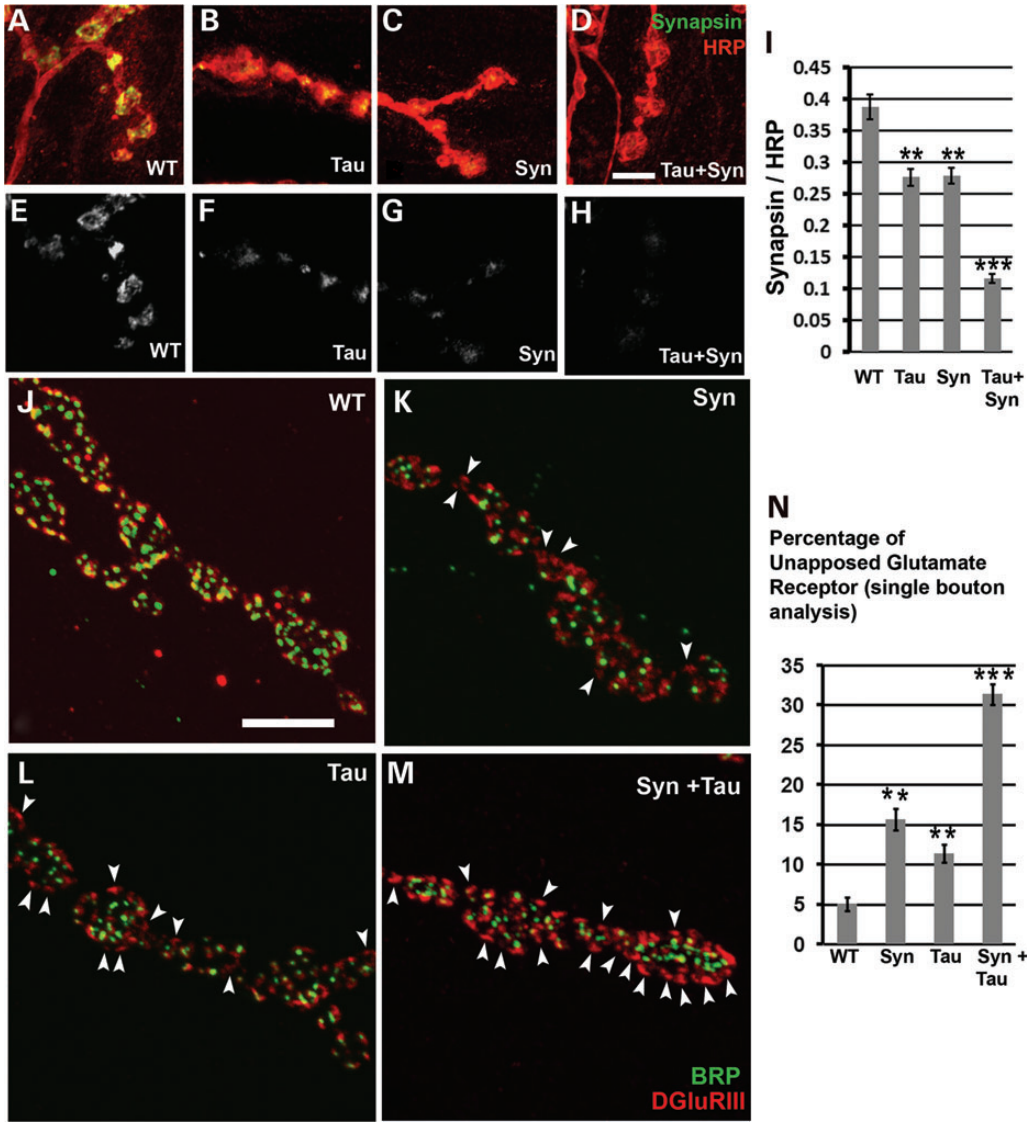

Figure 7. Coexpression of α-Syn and Tau decreases Synapsin in boutons and leads to synaptic apposition defects. (**A**–**D**) Confocal images of boutons at muscle 4 stained with anti-HRP (red; labels the presynaptic membrane) and 3C11 (green; anti-synapsin). (**E**–**H**) Confocal images of muscle 4 boutons showing the synapsin staining in gray scale. In comparison to the wild-type (OK6-GAL4/+) animals, there is a marked decrease in the levels of synapsin in the OK6-*GAL4/UAS-lacZ*; *UAS Syn*/+ and the OK6-*GAL4/UAS-Tau*; *UAS-lacZ*/+ animals. The decrease in synapsin is enhanced in the *OK6-GAL4/UAS-Tau*; *UAS-Syn*/+ animals. (**I**) Histogram showing synapsin levels. *Y*-axis, synapsin intensity/HRP intensity. N = total number of boutons of muscle four A3 hemisegment across 7–8 animals. Genotypes: (A) WT: OK6-GAL4-/+ ($N = 140$, *Y*-axis value = 0.388), (B) Syn: OK6-GAL4/UAS-lacZ; UAS-Syn/+ ($N = 144$, *Y*-axis value = 0.276), (C) Tau: OK6-GAL4/UAS-Tau; UAS-lacZ/+ ($N = 165$, *Y*-axis value = 0.278) and (D) Syn + Tau: OK6-GAL4/UAS-Tau; UAS-Syn/+ ($N = 154$, *Y*-axis value = 0.116). (**J**–**M**) Type 1b boutons of muscle four stained with antibodies to BRP (green) and the glutamate receptor DGluRIII (red). (J) BRP and glutamate receptor stained puncta either colocalize or are tightly apposed to each other at almost all synapses in wild-type animals (WT). In contrast, Syn (K) or Tau-expressing animals (L) show both colocalized BRP and DGluRIII as well as a few glutamate receptors unapposed to BRP (white arrowheads). DGluRIII unapposed to BRP is greatly increased in the Tau and Syn coexpressing animals. (**N**) A histogram showing the percentage of unapposed glutamate receptors in all four genotypes. *Y*-axis represents the percentage of unapposed glutamate receptors in a single bouton. N = total number of boutons of the muscle 4′s A3 hemisegment across 5–6 animals. Genotypes: (A) WT: OK6-GAL4/+ ($N = 100$, *Y*-axis value = 5.02), (B) Syn: OK6-GAL4/UAS-lacZ; UAS-Syn/+ ($N = 100$, *Y*-axis value = 15.69), (C) Tau: OK6-GAL4/UAS-Tau; UAS-lacZ/+ ($N = 100$, *Y*-axis value = 11.38), (D) Syn + Tau: OK6-GAL4/UAS-Tau/+; UAS-Syn/+ ($N = 105$, *Y*-axis value = 31.39). Values on the *Y*-axis represent mean ± SEM. $^{***}P < 0.001$; $^{**}P < 0.01$ using one-way ANOVA + Fisher LSD. Scale bar: 5 μm.

solubilization of proteins from fly head extracts using various buffers (phosphate-buffered saline (PBS), Triton X-100, SDS and urea) was performed to yield highly insoluble or membrane-bound proteins. Urea is known to solubilize hydrophobic membrane proteins in water (83,84). Tau decreased α-Syn in the PBS fraction (Fig. 9D and F, $P = 0.0023$) and increased its levels in the urea fraction (Fig. 9E and F, $P = 0.0047$). Thus, transgenic Tau decreased solubility of α-Syn and/or rendered it more membrane-bound *in vivo*.

DISCUSSION

GWAS have confirmed polymorphisms in SNCA and MAPT regions as common risk factors for sporadic PD. Missense

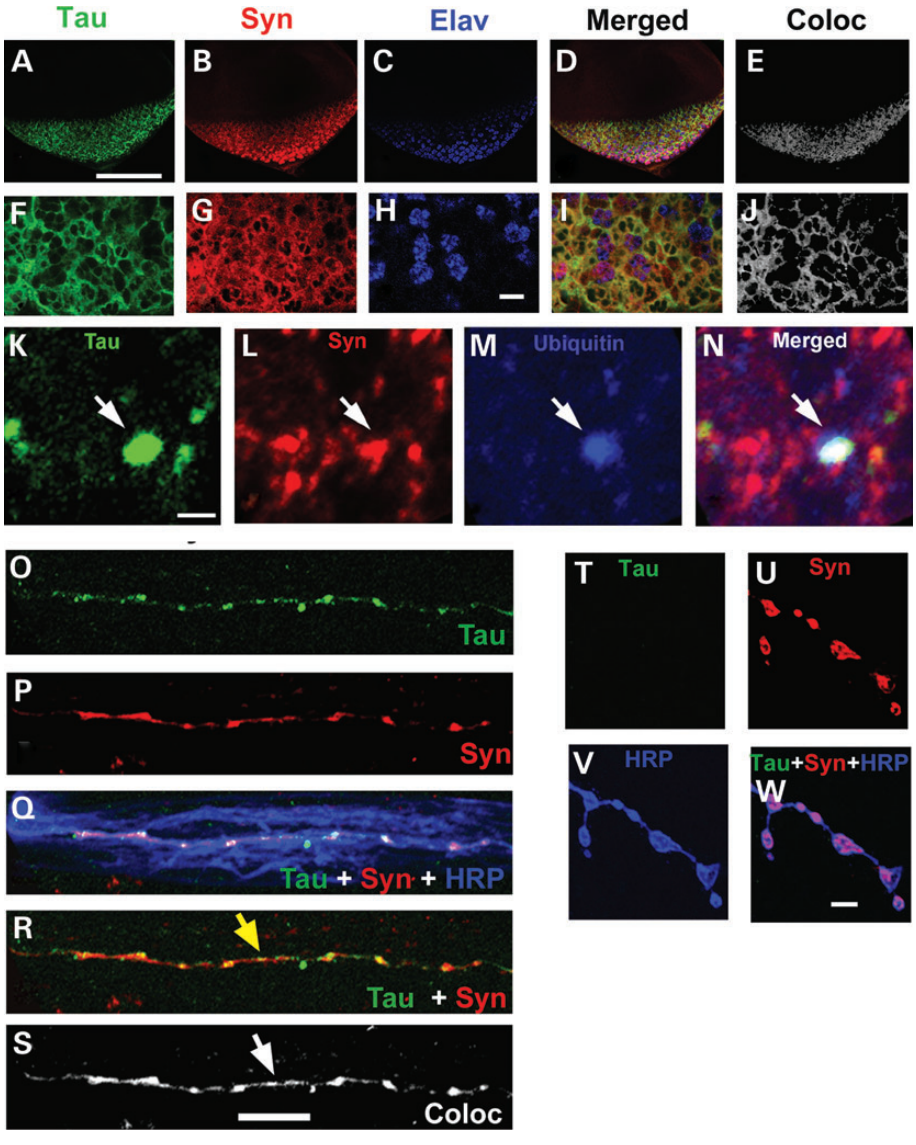

Figure 8. Localization of Tau and α-Syn in various tissue compartments of the double transgenics. (**A**–**J**) Syn and Tau colocalize in the cytoplasm of eye discs. (A–D, F–I) Confocal images of single optical sections of third instar larval eye discs from double transgenics stained with T46 (Tau; green). Syn (AB5038; red) and Elav (Blue). (F–J) Zoomed confocal images of single optical sections of eye discs from the same animals. (D, I) Merged confocal images of single optical section showing the staining pattern of the three antibodies. (E, J) Colocalized pixels (gray) of Tau and α-Syn in a single plane of the eye disc tissue using ImageJ, RG2B Coloc Plugin. (**K**–**N**) In random cytoplasmic regions α-Syn and Tau colocalize in ubiquitinated aggregates. (K–N) Confocal images of single sections stained with antibody against Tau (green, K), Syn (red, L) and ubiquitin (blue, M). Ubiquitin immunoreactive punctum is observed (blue) that is largely colocalized with Tau and Syn (N, white arrow). Genotype: GMR-GAL4/UAS-Tau 1.13; UAS Syn/+. (**O**–**S**) Synuclein and Tau colocalize in axons of motor neurons: single plane confocal image of segmental nerves of the OK6-GAL4/UAS-Tau; UAS-Syn/+ larvae stained with antibody against total Tau (green, O), Syn (red, P) and HRP (blue, Q). (R) Immunostaining of the OK6-GAL4/UAS-Tau; UAS-Syn/+ larvae shows colocalization of Tau and Syn in the axon (yellow arrow). (S) The colocalized pixels between Tau and Syn are highlighted using ImageJ, RG2B Colocalization PlugIn. Yellow and white arrows represent the intense colocalized signals in the axon of the segmental nerves in R and S. (**T**–**W**) Tau and Synuclein do not colocalize in boutons of the larval NMJ: single optical section of muscle four synapses stained with anti-Tau (green, T), anti-Syn (red, U) and HRP (blue, V). Syn is observed in synaptic boutons (U, W) but Tau is absent. Genotype: (O–W) OK6-GAL4/UAS-Tau; UAS-Syn/+. Scale bar: 100 μm (A–E), 6 μm (F–J), 1.5 μm (K–N), 10 μm (O–S) and 5 μm (T–W).

mutations A53T (85), A30P (86) and E46K (87), as well as genomic duplication and triplication of the SNCA locus (88,89) cause autosomal dominant familial PD. Frontotemporal dementia with parkinsonism linked to chromosome 17 (FTDP-17) is characterized by the abnormal deposition of tau (90). Since 1998, >25 mutations in MAPT have been associated with FTDP-17 (90). Tau mutations in FTDP-17 are missense or deletion mutations in the coding region or intronic mutations located close to the splice-donor site of the intron following the alternatively spliced exon 10. We examined the neurotoxic interaction of Tau and α-Syn in *Drosophila*. Our data have yielded insight into processes that are perturbed by this interaction and that culminate in neurodegeneration. Although others have attempted to unravel the basis of the neurotoxic α-Syn/Tau interaction, these efforts may not have uncovered the full spectrum of interactions that instigate neurodegeneration. We have focused on the influence of

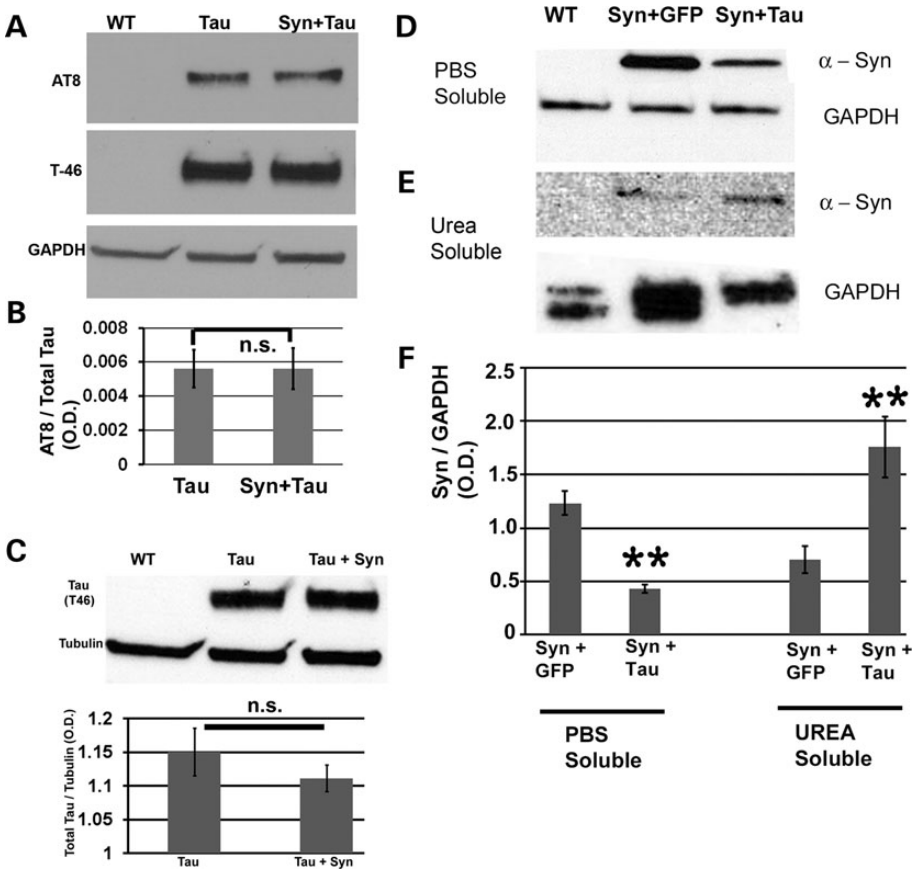

Figure 9. Mechanisms underlying Syn/Tau-mediated toxicity. Syn misexpression does not affect Tau phosphorylation at the AT8 epitope but Tau increases the formation of highly insoluble or membrane-associated Syn. (**A**) Immunoblot with phosphotau antibody (AT8), antibody against total Tau (T-46) and antibody against GAPDH (loading control). (**B**) Histograms representing relative phosphorylation levels of Tau in Tau alone and dual Tau/Syn transgenics. Results shown are derived from densitometry analysis of three separate blots. Each bar represents mean ± SEM ($N = 3$). P-value = 1; one-way ANOVA + Fisher LSD test). (**C**) Comparable levels of total Tau protein in Tau alone and dual Tau/Syn transgenics. Immunoblot using head extracts probed with T-46 and antibody against tubulin (loading control). Histograms representing relative levels of Tau in Tau alone and dual Tau/Syn transgenics. Results shown are derived from densitometric analysis and the value on the Y-axis is represented by OD [Tau] OD [Tubulin]. Each bar represents mean ± SEM ($N = 3$). P-value = 0.4; one-way ANOVA + Fisher multiple comparison test). Genotypes: (A–C) WT: GMR-GAL4/+, Tau: GMR-GAL4/+; *gl*-Tau/+, Syn + Tau: GMR-GAL4/+; *gl*-Tau/+; UAS-Syn/+. (**D**–**F**) Immunoblot using total Syn (4D6) and GAPDH antibodies (loading control) of PBS soluble (D) and urea soluble fractions (E) obtained after a serial extraction of proteins from fly head extracts in various buffers. Synuclein decreased in the PBS soluble fraction (D) and increased in the urea soluble fraction (E). (F) Histogram representing relative levels of Syn in the PBS soluble and urea soluble fractions of Syn + GFP and Syn + Tau transgenics. Results shown are derived from densitometric analysis of three separate blots. Each bar represents mean ± SEM ($N = 3$). P-value = 0.002 (PBS fraction) and 0.004 (urea fraction; one-way ANOVA + Fisher test). Genotypes: (D–F) WT: GMR-GAL4/+, Syn + GFP: GMR-GAL4/UAS-GFP; UAS-Syn/+, Syn + Tau: GMR-GAL4/UAS-Tau; UAS-Syn.

the α-Syn/Tau interaction on fundamental cellular processes including axonal transport and synaptic dysfunction. Misexpression of α-Syn increases a rough eye phenotype, consistent with its role as a modifier of Tau *in vivo*. Misexpression of α-Syn alone leads to dopaminergic cell loss by 6 weeks posteclosion, and Tau increases α-Syn-mediated dopaminergic cell loss. Misexpression of Tau alone does not affect DA cell count. These data demonstrate a synergistic neurotoxic interaction between Tau and α-Syn *in vivo*.

Immunohistochemistry of dual α-Syn/Tau eye discs shows colocalization. However, misexpression of α-Syn does not alter p-Tau levels as assessed using AT8 (91). The discrepancy of this result when compared with observations of Haggerty *et al.* (21) could be due to use of MPP^+ or the use of mutant α-Syn in the mouse work. The presence of neurotoxins such as MPP^+ (18–20) or paraquat (92) may aid in α-Syn-dependent Tau phosphorylation. A53T α-Syn increases Tau phosphorylation (82) and fibrillization (23). We previously demonstrated using a Tau modifier screen in *Drosophila* that modifying the severity of tau-induced toxicity does not require altering its phosphorylation state (25). We have also demonstrated dissociation between Tau phosphorylation and neurodegeneration in another context (91).

Since both Tau and α-Syn bind microtubules and actin, modulation of cytoskeletal architecture might contribute to neurotoxicity underlying the α-Syn/Tau interaction. Phalloidin and anti-tubulin staining of longitudinal retinal sections show highly disorganized rhabdomere shafts in dual Tau/α-Syn animals. The NMJ shows similar results with aberrant bouton morphology in α-Syn/Tau animals. Reversible coimmunoprecipitation, affinity chromatography and direct binding assays using radiolabelled proteins have confirmed the direct binding of α-Syn to Tau both *in vitro* and *in vivo* (19,21,93,94). We speculate that direct interaction of α-Syn and Tau modulates their affinity for tubulin and actin, thereby leading to cytoskeletal disorganization and destabilization. Coexpression of Tau and α-Syn increases axonal

accumulation of synaptic proteins DVGLUT and BRP. The extent of axonal traffic jams is highest in dual α-Syn/Tau transgenics, consistent with observations of others (31,49,95). A few DVGLUT aggregates are observed in α-Syn-expressing animals, but this result is not significantly different from wild type. Colocalization of Tau and α-Syn in the axons of the motor neurons implies a functional interaction of these proteins in blocking axonal transport. Since Tau and α-Syn bind both free tubulin and actin (39,65,96,97), in addition to binding to microtubules and the actin cytoskeleton, their interaction may disrupt axonal architecture, hinder attachment of cargo and motor proteins, and thereby disrupt axonal transport. An alternative explanation for Tau/α-Syn synergy invokes the ability of α-Syn to bind to microtubules (98) and Tau at its microtubule-binding site (93). We speculate that α-Syn binds to human Tau and aids its binding to microtubules. Increased binding of hypophosphorylable Tau (Tau^{AP} and Tau^{S11A}) to microtubules has deleterious effects on vesicle transport (49) and enhances adult eye phenotypes (91). Increased binding of Tau to microtubules will interfere with the normal binding of motor proteins leading to improper transport.

Synaptic dysfunction is an early event in the pathogenesis of AD (99) and PD (100). Synaptic dysfunction can be caused by abnormal synapse organization, which eventually compromises synaptic integrity and efficacy. Abnormalities in microtubule organization at the NMJ have been described in various neurodegenerative models in the fly (41,101,102). Abnormal microtubule organization in the boutons of dual α-Syn/Tau transgenics supports the hypothesis that defective synaptic cytoskeletal organization contributes to disease pathogenesis. We also saw some defects in the microtubule organization in the boutons of Tau misexpressing animals. This could explain the previously reported wide array of morphological defects observed at the synapse in tau transgenic flies (ON4R) (95). Another technique for assaying synaptic dysfunction is to look for changes in the expression and localization of synaptic proteins at the NMJ. BRP is required for structural integrity and function of synaptic active zones (52) and is altered in models of ALS8 (41). Shepherd and coworkers (72) observed abnormal distribution of synaptotagmin I in synaptic boutons in a fly tauopathy model. Dual α-Syn/Tau transgenics have decreased BRP puncta spanning the bouton area. Tau alone flies show some decline in BRP but much less when compared with dual transgenics. Due to impaired axonal transport in both the Tau/α-Syn and Tau alone flies, the amount of BRP that reaches synaptic terminals is likely to be insufficient. RNAi knockdown of BRP reduces quantal content and T bar formation at the larval NMJ (52), consistent with the hypothesis that BRP abnormalities in dual Tau/α-Syn dual transgenics lead to defects in synaptic transmission.

Drosophila synapsin maintains vesicle clustering over the periphery of the bouton (73) and is decreased in individual α-Syn and Tau transgenics. These data are consistent with the findings that α-Syn overexpression reduces synapsin 1 (68) and reminiscent of our observation that oligomeric Tau reduces levels of the synaptic vesicle-associated proteins synaptophysin and septin 11. Tau/α-Syn aggregates may sequester proteins, including synaptic proteins, thereby compromising their availability at the synapse. Alternatively, impaired transport may prevent efficient transfer of these proteins from the neuronal soma to presynaptic terminals. Coexpression of Tau and α-Syn lowers synapsin when compared with controls or single transgenics, likely due to enhanced axonal transport defects due to a direct interaction between axonal Tau and α-Syn, an indirect effect of Tau on α-Syn localization in synapses or sequestration of synaptic proteins by aggregates.

Coexpression of Tau and α-Syn also creates aberrant presynaptic/postsynaptic morphology in the larval NMJ. This may be due to impaired axonal transport as a direct effect of the α-Syn/Tau interaction or an indirect effect of Tau on the α-Syn localized in the presynaptic terminals. α-Syn associates with lipid rafts (103), interacts with membrane lipids to form toxic oligomers (104–106) and affects membrane bilayer structure and stability (107). Microtubule organization is more abnormal in boutons of the dual Tau/α-Syn animals. *In vitro* and *in vivo* experiments have demonstrated that tubulin seeds α-Syn fibril formation (108), and inhibiting microtubule assembly stimulates α-Syn aggregation (109). Microtubule disorganization in synaptic boutons may trigger α-Syn aggregation. These aggregates on binding to the lipid membranes may destabilize them, leading to the collapse of tight pre- and postsynaptic apposition. This explanation is partly supported by our biochemical results that show increased insoluble/membrane-associated α-Syn in the presence of Tau *in vivo*.

In summary, this work has helped to uncover aberrant cytoskeletal organization, axonal transport and synaptic architecture underlying neuronal dysfunction due to synergistic toxicity of α-Syn and Tau *in vivo*. Coaggregation of Tau and α-Syn, as well as Tau-mediated decreases in α-Syn solubility, are likely to lie at the root of these changes in axonal and synaptic morphology. These findings provide mechanistic insights into the synergistic interactions between the SNCA and MAPT loci which are likely to play an important role in the pathogenesis of sporadic idiopathic PD.

MATERIALS AND METHODS

Fly stocks and genetics

Flies were reared and maintained at 25°C on Jazzmix medium (Applied Scientific, Pittsburgh, PA, USA). All crosses were maintained under similar conditions. The GMR-GAL4 transgene on the X-chromosome (110) was placed in *trans* to the *gl*-tau line (26) to generate GMR-GAL4; *gl*-tau/CyO flies (25). UAS-α-Syn and the recombined TH-GAL4/UAS- α-Syn stocks were the generous gift of Leo Pallanck (24). To maximize α-Syn expression in dopaminergic neurons, we used two copies each of the TH-GAL4 and the UAS-α-Syn transgenes. This combination has been shown to cause significant DA cell loss when compared with the one copy each counterpart (24).Various other UAS transgenic lines used in our investigation are: UAS-Tau-1.13 (91), UAS-lacZ and UAS-GFP (Bloomington Stock Center). The GAL4-driver lines used in our studies are: GMR-GAL4 on X and the second chromosome (eye specific), TH-GAL4 (DA neuron specific) (111), $elav^{C155}$-GAL4 (pan neuronal) (112), OK6-GAL4 (motor neuron specific) (113) and the $VGLUT^{OK371}$-GAL4 (motor neuron-specific line) (114). w^{1118} was crossed to the various GAL4 lines to generate the control animals.

Three-dimensional image construction

Thoracic-abdominal segments of flies 3–4 days posteclosion were glued onto a microscope slide with transparent nail polish. The head of the fly was positioned such that the right eye was facing the objective lens of the microscope and the left side of the head stuck to the nail polish. To more accurately quantitate retinal degeneration, we used a Nikon AZ100M microscope in combination with NIS-Elements AR 3.0 software (Nikon Instruments, Melville, NY, USA), which features an 'extended depth of focus' algorithm allowing for three-dimensional reconstruction of Z-stack planar images (27).

Immunohistochemistry

DA neuron staining

Dissection and immunohistochemistry staining of adult brain were carried out using modifications of published protocols (115,116). Briefly, aged flies were anesthetized, decapitated and their heads incubated in fixative (4% paraformaldehyde + PBS + 0.1% Triton X-100) on ice for 30 min. The heads were then dissected to remove the entire brain. Brains were then fixed in the same fixative for 2 h on ice. After fixation, brains were washed four times for 15 min each with wash buffer (0.1% PTX = PBS + 0.1% Triton X-100) before incubation in blocking buffer (PBS + 0.1% Triton X-100 + 5% goat serum) for 1 h at room temperature. Tissues were incubated with mouse anti-tyrosine hydroxylase antibody (1 : 100, Immunostar, Hudson, WA, USA) overnight at 4°C. This was followed by incubation with Alexafluor-conjugated anti-mouse secondary antibody (1:400, Invitrogen, Carlsbad, CA, USA) for 2 h at room temperature. Brains were washed four times for 15 min each in wash buffer and mounted on coverslips with Vectashield (Vector Laboratories, Burlingame, CA, USA).

Larval NMJ staining

Larvae were dissected and stained as described (117,118). In brief, wandering third instar larvae were dissected in cold PBS and fixed for 5–10 min in Bouin's fixative and washed three times for 5 min each in 0.1% PTX. The samples were then incubated in the primary antibody solution (primary of the desired dilution + 2% normal goat serum + 0.1% PTX) overnight at 4°C. Primary antibodies were rabbit anti-GluRIII (1:2500) (117) (a gift from Yogesh Wairkar), mouse anti-BRP (1:250, Developmental Studies Hybridoma Bank (DSHB), Iowa City, IA, USA), mouse anti-synapsin (1:50; 3C11, DSHB), rabbit anti-HRP (1:400; Sigma), mouse anti-Futsch (1:50; 22C10, DSHB) and rabbit anti-DVGLUT (1:10,000; a gift from Y. Wairkar; (119)). Following this, the tissues were washed with 0.1% PTX thrice for 5 min each before being incubated with the appropriate secondary antibody for 1 h at room temperature. Staining was visualized using Alexafluor secondary antibodies (Invitrogen; 1:1000) and the HRP Dylight (Invitrogen; 1:1000).

Whole-mount staining of the adult retina and third instar eye imaginal discs

Longitudinal retinal whole-mount preparations were made from 6- to 7-day-old adult females as described previously (120). The retinal samples were fixed in 4% paraformaldehyde + 0.1% PTX for 3 h on ice. After fixation, retinal tissues were washed four times with 0.1% PTX and incubated in blocking buffer (PTX + 5% goat serum) for 1 h at room temperature. Tissues were incubated with primary antibody E7 (mouse anti-tubulin; DSHB) overnight at 4°C. This was followed by four washes with 0.1% PTX and incubation with Alexa goat anti-mouse secondary antibody (1:400; Invitrogen) for 2 h at room temperature. Tissues were washed four times for 15 min each in 0.1% PTX and mounted on slides with Vectashield. For phalloidin staining, after blocking, retinal samples were incubated with Alexa 568-conjugated phalloidin (1:400; Invitrogen) at 4°C overnight. This was followed by four washes with 0.1% PTX before mounting in Vectashield.

For eye disc staining, tissues were fixed in 4% paraformaldehyde in PTX for 2 h on ice. Washing and blocking were done as for adult retina. Tissues were incubated with rabbit anti cleaved caspase-3 (1:100; Cell Signaling Technology), mouse anti-Tau (Tau5, 1: 300; Invitrogen), rabbit anti-α-Syn (AB 5038, 1:400; Millipore), rat anti-Elav (7E8A10, 1:20; DSHB), mouse anti-α-Syn (4D6, 1:400; Covance), chicken anti-Tau (1:150; Neuromics) or rabbit anti-ubiquitin (1:200; Abcam) overnight at 4°C. This was followed by four washes with 0.1% PTX and incubation with goat Alexa-conjugated secondary antibody against the appropriate species (1:400; Invitrogen) for 2 h at room temperature. The tissues were washed in 0.1% PTX and mounted in Vectashield.

Behavior

Adult males 7 days posteclosion were selected for behavioral analysis. A single fly was placed in an empty vial. The fly was gently knocked down to the bottom of tube and allowed 10 s to climb up to the vial top. The distance travelled by individual flies in a 10 s time frame was measured. Five trials were run for each individual fly and the average of the five measurements was taken for statistical analysis. All analyses were performed with the experimenter blinded to genotype. Graphical and statistical analyses were performed using SigmaPlot 9.0 and SigmaStat 3.1 (Systat, San Jose, CA, USA).

Immunoblots

Freshly eclosed adult flies were collected and heads were dissected and homogenized in a lysis buffer consisting of 10 mM Tris–Cl (pH 7.4) + NaCl (0.8 M) + EGTA (1 mM, pH 8.0) + 10% sucrose + protease inhibitor cocktail and phosphatase inhibitor cocktail (Roche Applied Science, Indianapolis, IN, USA). Extracts were mixed with SDS sample buffer and separated by 10% SDS–PAGE. Proteins were transferred to nitrocellulose membranes, blocked in 5% (w/v) non-fat dried milk in Tris-buffered saline + 0.1% Tween 20 and immunoblotted using the following antibodies: T46 (Invitrogen; 1:1000), 4D6 (Covance; 1:1000) and anti-GAPDH (ProScience; 1:1000). The membranes were incubated with peroxidase-labeled anti-mouse or anti-rabbit IgG and signals were detected using chemiluminescence. Films derived from immunoblots were scanned using a Konica SRX—101A Tabletop X-Ray film processor. Densities of bands were measured using NIH ImageJ. Graphical and statistical analyses were performed using SigmaPlot 9.0 and SigmaStat 3.1 (Systat).

To derive highly insoluble or membrane-associated proteins, we performed a serial extraction of proteins in various buffers. Five hundred fly heads for each of the various genotypes were homogenized in PBS and centrifuged at 16 000*g* for 5 min. The pellet collected was homogenized in 2% Triton X-100 and vortexed. The pellet acquired from this step was redissolved in 2% SDS. The samples were vortexed again, and the pellet was dissolved in 2 M urea and incubated at room temperature overnight. The final extract of this solution was collected, mixed with SDS sample buffer and separated by 10% SDS–PAGE.

Image analysis and quantitation

Samples were imaged using a Zeiss LSM 510 Meta confocal microscope. For comparisons of fluorescence intensities across genotypes, samples from different genotypes were dissected and fixed identically and imaged under precisely identical conditions (identical exposures and light intensities) and in succession. For all data, images were taken at maximal brightness while avoiding saturation. Images were analyzed using LSM Image browser (for Z-stack processing) and NIH ImageJ software (quantitation). The experimenter was blinded to genotypes during both imaging and analysis. Statistical analysis was performed using one-way ANOVA for comparison of samples within an experimental group. All histograms and measurements are shown as mean ± SEM.

Quantification of cleaved caspase-3 immunoreactivity was performed by analyzing individual confocal Z-series using ImageJ version 1.46. After background correction, color depth reduction to 8 bits, and adjustment of the detection threshold, automated quantification was performed with the 'analyze particles' function using a size of $>6\ \mu m^2$ parameter. The total number of particles was scored automatically and divided by the total area of the eye imaginal disc (calculated using the ImageJ Analyze, measure tool).

The DA cell count was performed as described previously (121). Briefly, each brain was scanned using optical sections covering an area that included DA neurons of the DL clusters. Each brain was analyzed with the examiner blinded to the genotype. The collected Z-series from each brain were then projected into a three-dimensional animation using the Zeiss LSM Image browser Projection tool or 3D projection tool under the Stacks option in ImageJ to precisely quantitate DA neuron numbers. We defined neuronal loss as a complete loss of somatic TH staining. To avoid confocal settings in different batches of samples that might artificially affect data interpretation, age-matched brains from different genotypes were examined simultaneously.

Microtubule disorganization at the larval NMJ was assayed as described previously (41). This assay has also been reported as microtubule unbundling assay (42). Type1b boutons from hemisegments of muscle 4 (A2, A3 and A4) were scored based on the pattern of their Futsch staining. Boutons with splayed, diffuse/punctate or filled Futsch staining were scored as abnormal unbundled boutons, in contrast to boutons with filamentous, thread-like staining patterns. An index of microtubule disorganization was calculated by dividing the total number of abnormal boutons by the total number of boutons counted at the NMJ (abnormal boutons/(abnormal + normal boutons)).

For analysis of axonal transport, the intensity of BRP and HRP were measured in the axonal area in segments A3 and A4 (proximal end of the axon), using the ImageJ Analyze, Measure RGB plugin. The index of axonal transport defect was calculated by dividing the value of (BRP intensity/HRP intensity) by the area of the axon ((BRP intensity/HRP intensity)/area of axon in the A3–A4 segment). For quantification of axonal traffic jams, automated counting of the number of DVGLUT-positive aggregates of $>1.68\ \mu m^2$ was carried out. Alternatively, using the ImageJ background correction, color depth reduction to 8 bits and adjustment of the detection threshold, automated quantification was performed with the 'analyze particles' function with a size of $>1.68\ \mu m^2$ parameter to quantitate DVGLUT-immunoreactive traffic jams. The total number of these DVGLUT-positive aggregates was quantitated every 100 μm axonal length in the distal part (A5–A6 segment) of the segmental nerves.

Quantification of apposition defects at the resolution of the single bouton was adapted from the method reported by DiAntonio and colleagues (122). Briefly, wandering third instar larvae were stained with antibodies to BRP, DGluRIII (117) and HRP (123). All three markers were imaged at maximal brightness without the sample being saturated. The boundaries of the synaptic terminal were identified based on HRP staining to avoid inclusion of receptors and active zones from innervations other than motor neuron 4 1b prior to punctum counting. Next, active zone puncta apposed to receptor puncta were counted. Because an active zone punctum is apposed to a single glutamate receptor punctum, glutamate receptor counts were calculated as the number of apposed active zone puncta added to the number of unapposed glutamate receptor puncta. An unapposed glutamate receptor was defined as the receptor spot that occurred either in the absence of any nearby active zones or in rare cases with a small area of overlap with an adjacent active zone. Unapposed receptor puncta were divided by the total number of receptor puncta to determine the percent of unapposed glutamate receptors at the NMJ.

The analysis of changes in BRP was adapted from our previous work (41). We manually counted the total number of BRP puncta in a single type 1b bouton of the muscle 4 A3 NMJ and then divided the value by the total area of the bouton (number of BRP puncta in a single bouton/area of the bouton). For detection of changes in synapsin, ImageJ's Analyze, Measure RGB plugin was used. Using this plugin, intensities of synapsin and HRP were measured in single Type 1b boutons of the muscle 4 A3 NMJ. The quantitative index of synapsin levels was calculated by dividing the synapsin intensity by the HRP intensity.

SUPPLEMENTARY MATERIAL

Supplementary Material is available at *HMG* online.

ACKNOWLEDGEMENTS

We thank Leo Pallanck for providing us with the UAS-α-Syn transgenic flies, Yogi Wairkar for providing DVGLUT and GluRIII antibodies and the OK6-GAL4 line, Marie-Francoise Chesselet and David Krantz for helpful discussions and Jackson lab members for critically reading the manuscript. We also thank Adriana Paulucci and the Optical Microscopy Core at UTMB for assistance with confocal microscopy.

Conflict of Interest statement. None declared.

FUNDING

This research was supported by the National Institute of Health/NIH (P01 ES016732 to Marie-Francoise Chesselet), the Mitchell Foundation and the Cullen Trust for Heath Care.

REFERENCES

1. Morishima-Kawashima, M., Hasegawa, M., Takio, K., Suzuki, M., Yoshida, H., Watanabe, A., Titani, K. and Ihara, Y. (1995) Hyperphosphorylation of tau in PHF. *Neurobiol. Aging*, **16**, 365–371.
2. Johnson, G.V. and Bailey, C.D. (2002) Tau, where are we now? *J. Alz. Dis.*, **4**, 375–398.
3. Cookson, M.R. (2005) The biochemistry of Parkinson's disease. *Annu. Rev. Biochem.*, **74**, 29–52.
4. Wersinger, C. and Sidhu, A. (2005) Disruption of the interaction of α-synuclein with microtubules enhances cell surface recruitment of the dopamine transporter. *Biochemistry*, **44**, 13612–13624.
5. Hamilton, R.L. (2000) Lewy bodies in Alzheimer's disease: a neuropathological review of 145 cases using α-synuclein immunohistochemistry. *Brain Pathol.*, **10**, 378–384.
6. Kotzbauer, P.T., Trojanowski, J.Q. and Lee, V.M. (2001) Lewy body pathology in Alzheimer's disease. *J. Mol. Neurosci.*, **17**, 225–232.
7. Arai, Y., Yamazaki, M., Mori, O., Muramatsu, H., Asano, G. and Katayama, Y. (2001) α-synuclein-positive structures in cases with sporadic Alzheimer's disease: morphology and its relationship to tau aggregation. *Brain Res.*, **888**, 287–296.
8. Hishikawa, N., Hashizume, Y., Ujihira, N., Okada, Y., Yoshida, M. and Sobue, G. (2003) α-Synuclein-positive structures in association with diffuse neurofibrillary tangles with calcification. *Neuropath. Appl. Neurobiol.*, **29**, 280–287.
9. Popescu, A., Lippa, C.F., Lee, V.M. and Trojanowski, J.Q. (2004) Lewy bodies in the amygdala: increase of α-synuclein aggregates in neurodegenerative diseases with tau-based inclusions. *Arch. Neurol.*, **61**, 1915–1919.
10. Trembath, Y., Rosenberg, C., Ervin, J.F., Schmechel, D.E., Gaskell, P., Pericak-Vance, M., Vance, J. and Hulette, C.M. (2003) Lewy body pathology is a frequent co-pathology in familial Alzheimer's disease. *Acta Neuropathol.*, **105**, 484–488.
11. Lippa, S.M., Lippa, C.F. and Mori, H. (2005) α-synuclein aggregation in pathological aging and Alzheimer's disease: the impact of beta-amyloid plaque level. *Am. J. Alz. Dem.*, **20**, 315–318.
12. Lippa, C.F., Schmidt, M.L., Lee, V.M. and Trojanowski, J.Q. (1999) Antibodies to α-synuclein detect Lewy bodies in many Down's syndrome brains with Alzheimer's disease. *Ann. Neurol.*, **45**, 353–357.
13. Arima, K., Hirai, S., Sunohara, N., Aoto, K., Izumiyama, Y., Ueda, K., Ikeda, K. and Kawai, M. (1999) Cellular co-localization of phosphorylated tau- and NACP/α-synuclein-epitopes in Lewy bodies in sporadic Parkinson's disease and in dementia with Lewy bodies. *Brain Res.*, **843**, 53–61.
14. Ishizawa, T., Mattila, P., Davies, P., Wang, D. and Dickson, D.W. (2003) Colocalization of tau and α-synuclein epitopes in Lewy bodies. *J. Neuropathol. Exp. Neurol.*, **62**, 389–397.
15. Edwards, T.L., Scott, W.K., Almonte, C., Burt, A., Powell, E.H., Beecham, G.W., Wang, L., Zuchner, S., Konidari, I., Wang, G. *et al.* (2010) Genome-wide association study confirms SNPs in SNCA and the MAPT region as common risk factors for Parkinson disease. *Ann. Hum. Genet.*, **74**, 97–109.
16. Simon-Sanchez, J., Schulte, C., Bras, J.M., Sharma, M., Gibbs, J.R., Berg, D., Paisan-Ruiz, C., Lichtner, P., Scholz, S.W., Hernandez, D.G. *et al.* (2009) Genome-wide association study reveals genetic risk underlying Parkinson's disease. *Nat. Genet.*, **41**, 1308–1312.
17. Devine, M.J. and Lewis, P.A. (2008) Emerging pathways in genetic Parkinson's disease: tangles, Lewy bodies and LRRK2. *FEBS J.*, **275**, 5748–5757.
18. Duka, T. and Sidhu, A. (2006) The neurotoxin, MPP^+, induces hyperphosphorylation of Tau, in the presence of α-synuclein, in SH-SY5Y neuroblastoma cells. *Neurotox. Res.*, **10**, 1–10.
19. Duka, T., Rusnak, M., Drolet, R.E., Duka, V., Wersinger, C., Goudreau, J.L. and Sidhu, A. (2006) α-synuclein induces hyperphosphorylation of tau in the MPTP model of parkinsonism. *FASEB J.*, **20**, 2302–2312.
20. Duka, T., Duka, V., Joyce, J.N. and Sidhu, A. (2009) α-Synuclein contributes to GSK-3β-catalyzed tau phosphorylation in Parkinson's disease models. *FASEB J.*, **23**, 2820–2830.
21. Haggerty, T., Credle, J., Rodriguez, O., Wills, J., Oaks, A.W., Masliah, E. and Sidhu, A. (2011) Hyperphosphorylated tau in an α-synuclein-overexpressing transgenic model of Parkinson's disease. *Eur. J. Neurosci.*, **33**, 1598–1610.
22. Giasson, B.I., Forman, M.S., Higuchi, M., Golbe, L.I., Graves, C.L., Kotzbauer, P.T., Trojanowski, J.Q. and Lee, V.M. (2003) Initiation and synergistic fibrillization of tau and α-synuclein. *Science*, **300**, 636–640.
23. Kotzbauer, P.T., Giasson, B.I., Kravitz, A.V., Golbe, L.I., Mark, M.H., Trojanowski, J.Q. and Lee, V.M. (2004) Fibrillization of α-synuclein and tau in familial Parkinson's disease caused by the A53T α-synuclein mutation. *Exp. Neurol.*, **187**, 279–288.
24. Trinh, K., Moore, K., Wes, P.D., Muchowski, P.J., Dey, J., Andrews, L. and Pallanck, L.J. (2008) Induction of the phase II detoxification pathway suppresses neuron loss in *Drosophila* models of Parkinson's disease. *J. Neurosci.*, **28**, 465–472.
25. Ambegaokar, S.S. and Jackson, G.R. (2011) Functional genomic screen and network analysis reveal novel modifiers of tauopathy dissociated from tau phosphorylation. *Hum. Mol. Genet.*, **20**, 4947–4977.
26. Jackson, G.R., Wiedau-Pazos, M., Sang, T.K., Wagle, N., Brown, C.A., Massachi, S. and Geschwind, D.H. (2002) Human wild-type tau interacts with wingless pathway components and produces neurofibrillary pathology in *Drosophila*. *Neuron*, **34**, 509–519.
27. Ambegaokar, S.S. and Jackson, G.R. (2010) Interaction between eye pigment genes and tau-induced neurodegeneration in *Drosophila melanogaster*. *Genetics*, **186**, 435–442.
28. Fan, Y., Lee, T.V., Xu, D., Chen, Z., Lamblin, A.F., Steller, H. and Bergmann, A. (2010) Dual roles of Drosophila p53 in cell death and cell differentiation. *Cell Death Diff.*, **17**, 912–921.
29. Kato, K., Awasaki, T. and Ito, K. (2009) Neuronal programmed cell death induces glial cell division in the adult *Drosophila* brain. *Development*, **136**, 51–59.
30. Betz, A., Ryoo, H.D., Steller, H. and Darnell, J.E. Jr. (2008) STAT92E is a positive regulator of *Drosophila* inhibitor of apoptosis 1 (DIAP/1) and protects against radiation-induced apoptosis. *Proc. Natl. Acad. Sci. USA*, **105**, 13805–13810.
31. Mudher, A., Shepherd, D., Newman, T.A., Mildren, P., Jukes, J.P., Squire, A., Mears, A., Drummond, J.A., Berg, S., MacKay, D. *et al.* (2004) GSK-3β inhibition reverses axonal transport defects and behavioural phenotypes in *Drosophila*. *Mol. Psych.*, **9**, 522–530.
32. Alonso, A.D., Zaidi, T., Novak, M., Barra, H.S., Grundke-Iqbal, I. and Iqbal, K. (2001) Interaction of tau isoforms with Alzheimer's disease abnormally hyperphosphorylated tau and in vitro phosphorylation into the disease-like protein. *J. Biol. Chem.*, **276**, 37967–37973.
33. Abraha, A., Ghoshal, N., Gamblin, T.C., Cryns, V., Berry, R.W., Kuret, J. and Binder, L.I. (2000) C-terminal inhibition of tau assembly in vitro and in Alzheimer's disease. *J. Cell Sci.*, **113**, 3737–3745.
34. Jeannotte, A.M. and Sidhu, A. (2008) Regulated interactions of the norepineprhine transporter by the actin and microtubule cytoskeletons. *J. Neurochem.*, **105**, 1668–1682.
35. Kotani, S., Nishida, E., Kumagai, H. and Sakai, H. (1985) Calmodulin inhibits interaction of actin with MAP2 and Tau, two major microtubule-associated proteins. *J. Biol. Chem.*, **260**, 10779–10783.
36. Correas, I., Padilla, R. and Avila, J. (1990) The tubulin-binding sequence of brain microtubule-associated proteins, tau and MAP-2, is also involved in actin binding. *Biochem. J.*, **269**, 61–64.
37. Moraga, D.M., Nunez, P., Garrido, J. and Maccioni, R.B. (1993) A tau fragment containing a repetitive sequence induces bundling of actin filaments. *J. Neurochem.*, **61**, 979–986.
38. Henriquez, J.P., Cross, D., Vial, C. and Maccioni, R.B. (1995) Subpopulations of tau interact with microtubules and actin filaments in various cell types. *Cell Biochem. Funct.*, **13**, 239–250.
39. He, H.J., Wang, X.S., Pan, R., Wang, D.L., Liu, M.N. and He, R.Q. (2009) The proline-rich domain of tau plays a role in interactions with actin. *BMC Cell Biol.*, **10**, 81.
40. Hummel, T., Krukkert, K., Roos, J., Davis, G. and Klambt, C. (2000) *Drosophila* Futsch/22C10 is a MAP1B-like protein required for dendritic and axonal development. *Neuron*, **26**, 357–370.

41. Ratnaparkhi, A., Lawless, G.M., Schweizer, F.E., Golshani, P. and Jackson, G.R. (2008) A *Drosophila* model of ALS: human ALS-associated mutation in VAP33A suggests a dominant negative mechanism. *PLoS ONE*, **3**, e2334.
42. Viquez, N.M., Li, C.R., Wairkar, Y.P. and DiAntonio, A. (2006) The B' protein phosphatase 2A regulatory subunit well-rounded regulates synaptic growth and cytoskeletal stability at the *Drosophila* neuromuscular junction. *J. Neurosci.*, **26**, 9293–9303.
43. Pennetta, G., Hiesinger, P.R., Fabian-Fine, R., Meinertzhagen, I.A. and Bellen, H.J. (2002*) Drosophila* VAP-33A directs bouton formation at neuromuscular junctions in a dosage-dependent manner. *Neuron*, **35**, 291–306.
44. Packard, M., Koo, E.S., Gorczyca, M., Sharpe, J., Cumberledge, S. and Budnik, V. (2002) The Drosophila Wnt, wingless, provides an essential signal for pre- and postsynaptic differentiation. *Cell*, **111**, 319–330.
45. Coleman, M. (2005) Axon degeneration mechanisms: commonality amid diversity. *Nat. Rev. Neurosci.*, **6**, 889–898.
46. Ebneth, A., Godemann, R., Stamer, K., Illenberger, S., Trinczek, B. and Mandelkow, E. (1998) Overexpression of tau protein inhibits kinesin-dependent trafficking of vesicles, mitochondria, and endoplasmic reticulum: implications for Alzheimer's disease. *J. Cell Biol.*, **143**, 777–794.
47. Nuydens, R., Van Den Kieboom, G., Nolten, C., Verhulst, C., Van Osta, P., Spittaels, K., Van den Haute, C., De Feyter, E., Geerts, H. and Van Leuven, F. (2002) Coexpression of GSK-3β corrects phenotypic aberrations of dorsal root ganglion cells, cultured from adult transgenic mice overexpressing human protein tau. *Neurobiol. Dis.*, **9**, 38–48.
48. Stamer, K., Vogel, R., Thies, E., Mandelkow, E. and Mandelkow, E.M. (2002) Tau blocks traffic of organelles, neurofilaments, and APP vesicles in neurons and enhances oxidative stress. *J. Cell Biol.*, **156**, 1051–1063.
49. Talmat-Amar, Y., Arribat, Y., Redt-Clouet, C., Feuillette, S., Bouge, A.L., Lecourtois, M. and Parmentier, M.L. (2011) Important neuronal toxicity of microtubule-bound tau in vivo in *Drosophila*. *Hum. Mol. Genet.*, **20**, 3738–3745.
50. Hurd, D.D. and Saxton, W.M. (1996) Kinesin mutations cause motor neuron disease phenotypes by disrupting fast axonal transport in *Drosophila*. *Genetics*, **144**, 1075–1085.
51. Liu, Z., Huang, Y., Zhang, Y., Chen, D. and Zhang, Y.Q. (2011) *Drosophila* Acyl-CoA synthetase long-chain family member 4 regulates axonal transport of synaptic vesicles and is required for synaptic development and transmission. *J. Neurosci.*, **31**, 2052–2063.
52. Wagh, D.A., Rasse, T.M., Asan, E., Hofbauer, A., Schwenkert, I., Durrbeck, H., Buchner, S., Dabauvalle, M.C., Schmidt, M., Qin, G. *et al.* (2006) Bruchpilot, a protein with homology to ELKS/CAST, is required for structural integrity and function of synaptic active zones in *Drosophila*. *Neuron*, **49**, 833–844.
53. Horiuchi, D., Collins, C.A., Bhat, P., Barkus, R.V., Diantonio, A. and Saxton, W.M. (2007) Control of a kinesin-cargo linkage mechanism by JNK pathway kinases. *Curr. Biol.*, **17**, 1313–1317.
54. Schulz-Schaeffer, W.J. (2010) The synaptic pathology of α-synuclein aggregation in dementia with Lewy bodies, Parkinson's disease and Parkinson's disease dementia. *Acta Neuropathol.*, **120**, 131–143.
55. Kramer, M.L., Behrens, C. and Schulz-Schaeffer, W.J. (2008) Selective detection, quantification, and subcellular location of α-synuclein aggregates with a protein aggregate filtration assay. *BioTechniques*, **44**, 403–411.
56. Davidson, W.S., Jonas, A., Clayton, D.F. and George, J.M. (1998) Stabilization of α-synuclein secondary structure upon binding to synthetic membranes. *J. Biol. Chem.*, **273**, 9443–9449.
57. Jenco, J.M., Rawlingson, A., Daniels, B. and Morris, A.J. (1998) Regulation of phospholipase D2: selective inhibition of mammalian phospholipase D isoenzymes by α- and β-synucleins. *Biochemistry*, **37**, 4901–4909.
58. Bonini, N.M. and Giasson, B.I. (2005) Snaring the function of α-synuclein. *Cell*, **123**, 359–361.
59. Burre, J., Sharma, M., Tsetsenis, T., Buchman, V., Etherton, M.R. and Sudhof, T.C. (2010) α-synuclein promotes SNARE-complex assembly in vivo and in vitro. *Science*, **329**, 1663–1667.
60. Chandra, S., Gallardo, G., Fernandez-Chacon, R., Schluter, O.M. and Sudhof, T.C. (2005) α-synuclein cooperates with CSPα in preventing neurodegeneration. *Cell*, **123**, 383–396.
61. Darios, F., Ruiperez, V., Lopez, I., Villanueva, J., Gutierrez, L.M. and Davletov, B. (2010) α-synuclein sequesters arachidonic acid to modulate SNARE-mediated exocytosis. *EMBO Rep.*, **11**, 528–533.
62. Engelender, S., Kaminsky, Z., Guo, X., Sharp, A.H., Amaravi, R.K., Kleiderlein, J.J., Margolis, R.L., Troncoso, J.C., Lanahan, A.A., Worley, P.F. *et al.* (1999) Synphilin-1 associates with alpha-synuclein and promotes the formation of cytosolic inclusions. *Nat. Genet.*, **22**, 110–114.
63. Garcia-Reitbock, P., Anichtchik, O., Bellucci, A., Iovino, M., Ballini, C., Fineberg, E., Ghetti, B., Della Corte, L., Spano, P., Tofaris, G.K. *et al.* (2010) SNARE protein redistribution and synaptic failure in a transgenic mouse model of Parkinson's disease. *Brain*, **133**, 2032–2044.
64. Scott, D.A., Tabarean, I., Tang, Y., Cartier, A., Masliah, E. and Roy, S. (2010) A pathologic cascade leading to synaptic dysfunction in α-synuclein-induced neurodegeneration. *J. Neurosci.*, **30**, 8083–8095.
65. Sousa, V.L., Bellani, S., Giannandrea, M., Yousuf, M., Valtorta, F., Meldolesi, J. and Chieregatti, E. (2009) α-synuclein and its A30P mutant affect actin cytoskeletal structure and dynamics. *Mol. Biol. Cell*, **20**, 3725–3739.
66. Abeliovich, A., Schmitz, Y., Farinas, I., Choi-Lundberg, D., Ho, W.H., Castillo, P.E., Shinsky, N., Verdugo, J.M., Armanini, M., Ryan, A. *et al.* (2000) Mice lacking α display functional deficits in the nigrostriatal dopamine system. *Neuron*, **25**, 239–252.
67. Gureviciene, I., Gurevicius, K. and Tanila, H. (2007) Role of alpha-synuclein in synaptic glutamate release. *Neurobiol. Dis.*, **28**, 83–89.
68. Nemani, V.M., Lu, W., Berge, V., Nakamura, K., Onoa, B., Lee, M.K., Chaudhry, F.A., Nicoll, R.A. and Edwards, R.H. (2010) Increased expression of alpha-synuclein reduces neurotransmitter release by inhibiting synaptic vesicle reclustering after endocytosis. *Neuron*, **65**, 66–79.
69. Binder, L.I., Frankfurter, A. and Rebhun, L.I. (1985) The distribution of tau in the mammalian central nervous system. *J. Cell Biol.*, **101**, 1371–1378.
70. Thies, E. and Mandelkow, E.M. (2007) Missorting of tau in neurons causes degeneration of synapses that can be rescued by the kinase MARK2/Par-1. *J. Neurosci.*, **27**, 2896–2907.
71. Lasagna-Reeves, C.A., Castillo-Carranza, D.L., Sengupta, U., Clos, A.L., Jackson, G.R. and Kayed, R. (2011) Tau oligomers impair memory and induce synaptic and mitochondrial dysfunction in wild-type mice. *Mol. Neurodegener.*, **6**, 39.
72. Chee, F.C., Mudher, A., Cuttle, M.F., Newman, T.A., MacKay, D., Lovestone, S. and Shepherd, D. (2005) Over-expression of tau results in defective synaptic transmission in Drosophila neuromuscular junctions. *Neurobiol. Dis.*, **20**, 918–928.
73. Akbergenova, Y. and Bykhovskaia, M. (2010) Synapsin regulates vesicle organization and activity-dependent recycling at Drosophila motor boutons. *Neuroscience*, **170**, 441–452.
74. Wang, P., Yang, G., Mosier, D.R., Chang, P., Zaidi, T., Gong, Y.D., Zhao, N.M., Dominguez, B., Lee, K.F., Gan, W.B. *et al.* (2005) Defective neuromuscular synapses in mice lacking amyloid precursor protein (APP) and APP-like protein 2. *J. Neurosci.*, **25**, 1219–1225.
75. Iseki, E., Marui, W., Kosaka, K. and Ueda, K. (1999) Frequent coexistence of Lewy bodies and neurofibrillary tangles in the same neurons of patients with diffuse Lewy body disease. *Neurosci. Lett.*, **265**, 9–12.
76. Yogev, S., Schejter, E.D. and Shilo, B.Z. (2008) Drosophila EGFR signalling is modulated by differential compartmentalization of Rhomboid intramembrane proteases. *EMBO J.*, **27**, 1219–1230.
77. Haass, C. and Selkoe, D.J. (2007) Soluble protein oligomers in neurodegeneration: lessons from the Alzheimer's amyloid beta-peptide. *Nat. Rev. Mol. Cell Biol.*, **8**, 101–112.
78. Bruijn, L.I., Houseweart, M.K., Kato, S., Anderson, K.L., Anderson, S.D., Ohama, E., Reaume, A.G., Scott, R.W. and Cleveland, D.W. (1998) Aggregation and motor neuron toxicity of an ALS-linked SOD1 mutant independent from wild-type SOD1. *Science*, **281**, 1851–1854.
79. Forman, M.S., Trojanowski, J.Q. and Lee, V.M. (2004) Neurodegenerative diseases: a decade of discoveries paves the way for therapeutic breakthroughs. *Nat. Med.*, **10**, 1055–1063.
80. Soto, C., Estrada, L. and Castilla, J. (2006) Amyloids, prions and the inherent infectious nature of misfolded protein aggregates. *Trends Biochem. Sci.*, **31**, 150–155.
81. Orr, H.T. and Zoghbi, H.Y. (2007) Trinucleotide repeat disorders. *Annu. Rev. Neurosci.*, **30**, 575–621.
82. Wills, J., Credle, J., Haggerty, T., Lee, J.H., Oaks, A.W. and Sidhu, A. (2011) Tauopathic changes in the striatum of A53T alpha-synuclein mutant mouse model of Parkinson's disease. *PLoS ONE*, **6**, e17953.

83. Bowie, J.U. (2004) Membrane proteins: a new method enters the fold. *Proc. Natl. Acad. Sci. USA*, **101**, 3995–3996.
84. Molloy, M.P., Herbert, B.R., Walsh, B.J., Tyler, M.I., Traini, M., Sanchez, J.C., Hochstrasser, D.F., Williams, K.L. and Gooley, A.A. (1998) Extraction of membrane proteins by differential solubilization for separation using two-dimensional gel electrophoresis. *Electrophoresis*, **19**, 837–844.
85. Polymeropoulos, M.H., Lavedan, C., Leroy, E., Ide, S.E., Dehejia, A., Dutra, A., Pike, B., Root, H., Rubenstein, J., Boyer, R. *et al.* (1997) Mutation in the alpha-synuclein gene identified in families with Parkinson's disease. *Science*, **276**, 2045–2047.
86. Kruger, R., Kuhn, W., Muller, T., Woitalla, D., Graeber, M., Kosel, S., Przuntek, H., Epplen, J.T., Schols, L. and Riess, O. (1998) Ala30Pro mutation in the gene encoding alpha-synuclein in Parkinson's disease. *Nat. Genet.*, **18**, 106–108.
87. Zarranz, J.J., Alegre, J., Gomez-Esteban, J.C., Lezcano, E., Ros, R., Ampuero, I., Vidal, L., Hoenicka, J., Rodriguez, O., Atares, B. *et al.* (2004) The new mutation, E46K, of alpha-synuclein causes Parkinson and Lewy body dementia. *Ann. Neurol.*, **55**, 164–173.
88. Ibanez, P., Bonnet, A.M., Debarges, B., Lohmann, E., Tison, F., Pollak, P., Agid, Y., Durr, A. and Brice, A. (2004) Causal relation between alpha-synuclein gene duplication and familial Parkinson's disease. *Lancet*, **364**, 1169–1171.
89. Singleton, A.B., Farrer, M., Johnson, J., Singleton, A., Hague, S., Kachergus, J., Hulihan, M., Peuralinna, T., Dutra, A., Nussbaum, R. *et al.* (2003) alpha-Synuclein locus triplication causes Parkinson's disease. *Science*, **302**, 841.
90. Ingram, E.M. and Spillantini, M.G. (2002) Tau gene mutations: dissecting the pathogenesis of FTDP-17. *Trends Mol. Med.*, **8**, 555–562.
91. Chatterjee, S., Sang, T.K., Lawless, G.M. and Jackson, G.R. (2009) Dissociation of tau toxicity and phosphorylation: role of GSK-3beta, MARK and Cdk5 in a Drosophila model. *Hum. Mol. Genet.*, **18**, 164–177.
92. Wills, J., Credle, J., Oaks, A.W., Duka, V., Lee, J.H., Jones, J. and Sidhu, A. (2012) Paraquat, but not maneb, induces synucleinopathy and tauopathy in striata of mice through inhibition of proteasomal and autophagic pathways. *PLoS ONE*, **7**, e30745.
93. Jensen, P.H., Hager, H., Nielsen, M.S., Hojrup, P., Gliemann, J. and Jakes, R. (1999) α-synuclein binds to Tau and stimulates the protein kinase A-catalyzed tau phosphorylation of serine residues 262 and 356. *J. Biol. Chem.*, **274**, 25481–25489.
94. Benussi, L., Ghidoni, R., Paterlini, A., Nicosia, F., Alberici, A.C., Signorini, S., Barbiero, L. and Binetti, G. (2005) Interaction between tau and α-synuclein proteins is impaired in the presence of P301L tau mutation. *Exp. Cell Res.*, **308**, 78–84.
95. Ubhi, K.K., Shaibah, H., Newman, T.A., Shepherd, D. and Mudher, A. (2007) A comparison of the neuronal dysfunction caused by *Drosophila* tau and human tau in a *Drosophila* model of tauopathies. *Invert. Neurosci.*, **7**, 165–171.
96. Chau, M.F., Radeke, M.J., de Ines, C., Barasoain, I., Kohlstaedt, L.A. and Feinstein, S.C. (1998) The microtubule-associated protein tau cross-links to two distinct sites on each α and β tubulin monomer via separate domains. *Biochem.*, **37**, 17692–17703.
97. Zhou, R.M., Huang, Y.X., Li, X.L., Chen, C., Shi, Q., Wang, G.R., Tian, C., Wang, Z.Y., Jing, Y.Y., Gao, C. *et al.* (2010) Molecular interaction of α-synuclein with tubulin influences on the polymerization of microtubule in vitro and structure of microtubule in cells. *Mol. Biol. Rep.*, **37**, 3183–3192.
98. Alim, M.A., Ma, Q.L., Takeda, K., Aizawa, T., Matsubara, M., Nakamura, M., Asada, A., Saito, T., Kaji, H., Yoshii, M. *et al.* (2004) Demonstration of a role for α-synuclein as a functional microtubule-associated protein. *J. Alz. Dis.*, **6**, 435–442.
99. Selkoe, D.J. (2002) Alzheimer's disease is a synaptic failure. *Science*, **298**, 789–791.
100. Calabresi, P., Galletti, F., Saggese, E., Ghiglieri, V. and Picconi, B. (2007) Neuronal networks and synaptic plasticity in Parkinson's disease: beyond motor deficits. *Parkins. Rel. Dis.*, **13**, S259–S262.
101. Lee, S., Liu, H.P., Lin, W.Y., Guo, H. and Lu, B. (2010) LRRK2 kinase regulates synaptic morphology through distinct substrates at the presynaptic and postsynaptic compartments of the *Drosophila* neuromuscular junction. *J. Neurosci.*, **30**, 16959–16969.
102. Godena, V.K., Romano, G., Romano, M., Appocher, C., Klima, R., Buratti, E., Baralle, F.E. and Feiguin, F. (2011) TDP-43 regulates *Drosophila* neuromuscular junctions growth by modulating Futsch/MAP1B levels and synaptic microtubules organization. *PLoS ONE*, **6**, e17808.
103. Fortin, D.L., Troyer, M.D., Nakamura, K., Kubo, S., Anthony, M.D. and Edwards, R.H. (2004) Lipid rafts mediate the synaptic localization of α-synuclein. *J. Neurosci.*, **24**, 6715–6723.
104. Perlmutter, J.D., Braun, A.R. and Sachs, J.N. (2009) Curvature dynamics of α-synuclein familial Parkinson disease mutants: molecular simulations of the micelle- and bilayer-bound forms. *J. Biol. Chem.*, **284**, 7177–7189.
105. van Rooijen, B.D., Claessens, M.M. and Subramaniam, V. (2010) Membrane interactions of oligomeric α-synuclein: potential role in Parkinson's disease. *Curr. Prot. Pept. Sci.*, **11**, 334–342.
106. van Rooijen, B.D., Claessens, M.M. and Subramaniam, V. (2010) Membrane permeabilization by oligomeric α-synuclein: in search of the mechanism. *PLoS ONE*, **5**, e14292.
107. Zhu, M., Li, J. and Fink, A.L. (2003) The association of α-synuclein with membranes affects bilayer structure, stability, and fibril formation. *J. Biol. Chem.*, **278**, 40186–40197.
108. Alim, M.A., Hossain, M.S., Arima, K., Takeda, K., Izumiyama, Y., Nakamura, M., Kaji, H., Shinoda, T., Hisanaga, S. and Ueda, K. (2002) Tubulin seeds α-synuclein fibril formation. *J. Biol. Chem.*, **277**, 2112–2117.
109. Kim, M., Jung, W., Lee, I.H., Bhak, G., Paik, S.R. and Hahn, J.S. (2008) Impairment of microtubule system increases α-synuclein aggregation and toxicity. *Biochem. Biophys. Res. Commun.*, **365**, 628–635.
110. Takahashi, Y., Hirose, F., Matsukage, A. and Yamaguchi, M. (1999) Identification of three conserved regions in the DREF transcription factors from *Drosophila melanogaster* and *Drosophila virilis*. *Nucleic Acids Res.*, **27**, 510–516.
111. Friggi-Grelin, F., Coulom, H., Meller, M., Gomez, D., Hirsh, J. and Birman, S. (2003) Targeted gene expression in *Drosophila* dopaminergic cells using regulatory sequences from tyrosine hydroxylase. *J. Neurobiol.*, **54**, 618–627.
112. Lin, D.M. and Goodman, C.S. (1994) Ectopic and increased expression of Fasciclin II alters motoneuron growth cone guidance. *Neuron*, **13**, 507–523.
113. Aberle, H., Haghighi, A.P., Fetter, R.D., McCabe, B.D., Magalhaes, T.R. and Goodman, C.S. (2002) wishful thinking encodes a BMP type II receptor that regulates synaptic growth in Drosophila. *Neuron*, **33**, 545–558.
114. Keller, L.C., Cheng, L., Locke, C.J., Muller, M., Fetter, R.D. and Davis, G.W. (2011) Glial-derived prodegenerative signaling in the *Drosophila* neuromuscular system. *Neuron*, **72**, 760–775.
115. Jhaveri, D., Sen, A. and Rodrigues, V. (2000) Mechanisms underlying olfactory neuronal connectivity in *Drosophila*: the atonal lineage organizes the periphery while sensory neurons and glia pattern the olfactory lobe. *Dev. Biol.*, **226**, 73–87.
116. Wu, J.S. and Luo, L. (2006) A protocol for dissecting *Drosophila melanogaster* brains for live imaging or immunostaining. *Nat. Prot.*, **1**, 2110–2115.
117. Marrus, S.B., Portman, S.L., Allen, M.J., Moffat, K.G. and DiAntonio, A. (2004) Differential localization of glutamate receptor subunits at the *Drosophila* neuromuscular junction. *J. Neurosci.*, **24**, 1406–1415.
118. Wairkar, Y.P., Fradkin, L.G., Noordermeer, J.N. and DiAntonio, A. (2008) Synaptic defects in a *Drosophila* model of congenital muscular dystrophy. *J. Neurosci.*, **28**, 3781–3789.
119. Daniels, R.W., Collins, C.A., Gelfand, M.V., Dant, J., Brooks, E.S., Krantz, D.E. and DiAntonio, A. (2004) Increased expression of the Drosophila vesicular glutamate transporter leads to excess glutamate release and a compensatory decrease in quantal content. *J. Neurosci.*, **24**, 10466–10474.
120. Sang, T.K., Li, C., Liu, W., Rodriguez, A., Abrams, J.M., Zipursky, S.L. and Jackson, G.R. (2005) Inactivation of *Drosophila* Apaf-1 related killer suppresses formation of polyglutamine aggregates and blocks polyglutamine pathogenesis. *Hum. Mol. Genet.*, **14**, 357–372.
121. Sang, T.K., Chang, H.Y., Lawless, G.M., Ratnaparkhi, A., Mee, L., Ackerson, L.C., Maidment, N.T., Krantz, D.E. and Jackson, G.R. (2007) A Drosophila model of mutant human parkin-induced toxicity demonstrates selective loss of dopaminergic neurons and dependence on cellular dopamine. *J. Neurosci.*, **27**, 981–992.
122. Viquez, N.M., Fuger, P., Valakh, V., Daniels, R.W., Rasse, T.M. and DiAntonio, A. (2009) PP2A and GSK-3beta act antagonistically to regulate active zone development. *J. Neurosci.*, **29**, 11484–11494.
123. Jan, L.Y. and Jan, Y.N. (1982) Antibodies to horseradish peroxidase as specific neuronal markers in *Drosophila* and in grasshopper embryos. *Proc. Natl. Acad. Sci. USA*, **79**, 2700–2704.